BROADband brain Network Estimation via Source Separation (BROAD-NESS)

Bonetti, L.[1,2,3], Fernández-Rubio, G.[1], Andersen, M. H.[1,4], Malvaso, C.[5], Carlomagno, F.[1,6], Testa, C.[5], Vuust, P.[1], Kringelbach, M. L.[1,2,3], Rosso, M. [1,7*]*

[1] Center for Music in the Brain, Department of Clinical Medicine, Aarhus University & The Royal Academy of Music, Aarhus/Aalborg, Denmark

[2] Centre for Eudaimonia and Human Flourishing, Linacre College, University of Oxford, Oxford, United Kingdom

[3] Department of Psychiatry, University of Oxford, Oxford, United Kingdom

[4] Department of Psychology and Behavioural Sciences, Aarhus University, Aarhus, Denmark

[5] Department of Physics and Astronomy, University of Bologna, Bologna, Italy

[6] Department of Education, Psychology, Communication, University of Bari Aldo Moro, Italy

[7] IPEM Institute for Systematic Musicology, Ghent University, Ghent, Belgium

*Corresponding authors: leonardo.bonetti@psych.ox.ac.uk mattia.rosso@clin.au.dk

ABSTRACT

This study presents BROADband brain Network Estimation via Source Separation (BROAD-NESS), a novel method tailored for event-related designs, leveraging magnetoencephalography's (MEG) high temporal and spatial resolution to identify dynamic brain networks without predefined regions. By applying principal component analysis (PCA) to source-reconstructed MEG data from 83 participants in a long-term musical sequence recognition task, BROAD-NESS captured event-related networks more effectively than traditional approaches, revealing two main networks that explained 88% of the variance. The first network, involving the auditory cortices and medial cingulate gyrus, was associated with continuous auditory processing. The second network, encompassing prefrontal and hippocampal regions, inferior temporal cortex, and insula, was linked to memory, confirmed predictions and prediction error processing. With limited computational demands and minimal assumptions, BROAD-NESS offers a powerful tool for studying event-related brain dynamics, enhancing understanding of memory-related networks in recognition of temporal sequences.

Keywords

Brain Networks, Event-Related Responses, Linear Decomposition, Neurophysiology, Principal Component Analysis

Introduction

Cognitive neuroscience seeks to explain how the brain processes stimuli and performs cognitive tasks during interactions with the external environment[1-4]. To investigate these processes, researchers often rely on event-related designs, where repeated stimuli or tasks allow for tracking brain dynamics over time[5]. Crucially, high temporal resolution neurophysiological techniques, such as magnetoencephalography (MEG) and electroencephalography (EEG), are used to capture the rapid neural activity triggered by these events. However, interpreting event-related responses from scalp sensors is challenging due to the difficulty in linking these signals to specific brain sources (e.g., see[6]) as the recorded activity is a complex mixture of overlapping neural processes[6]. Therefore, developing robust methods to isolate distinct brain networks contributing to event-related responses is crucial for advancing our understanding of the brain mechanisms underlying perceptual and cognitive functioning in stimulus processing.

Most previous studies have relied on region-of-interest (ROI)-based approaches to examine brain sources, either by analysing the mere activation of individual ROIs or the changes in their connectivity following an event (e.g.[7]). This research has primarily focused on three types of analysis, built on ingenious yet often elaborated methods: (i) pairwise connectivity without directionality (e.g. Static Functional Connectivity [SFC] (e.g.[8]), Instantaneous Phase Synchronisation [IPS][9]), (ii) pairwise connectivity with directionality (e.g. Granger causality [GC][10], Transfer Entropy [TE][11], Partial Directed Coherence [PDC][12], Directed Transfer Function [DTF][13], Coherence and Phase Slope Index [PSI][14]) and (iii) estimation of functional properties of brain networks in a pre-defined set of ROIs or parcellation (e.g. Dynamic Causal Modelling [DCM][15], graph theory on functional connectivity matrices[16], Hidden Markov Model [HMM] e.g.[17], Leading Eigenvector Dynamics Analysis [LEiDA][18]). While ROI-based approaches have provided valuable insights, they are fundamentally limited. By focusing on predefined regions, they risk overlooking much of the information contained in the multivariate data. Additionally, they are often hypothesis-driven, requiring researchers to select specific regions for analysis in advance. As a result, ROI-based approaches may not fully leverage the high-dimensional data from neurophysiological recordings, suggesting that to fully exploit the richness of these datasets, it is crucial to avoid reducing the data before conducting network analyses.

A widely used alternative to ROIs-based approaches in cognitive neuroscience is multivariate pattern analysis (decoding), which operates on all available data, either at the sensor or the source level[19,20]. This method offers a means to classify experimental conditions by leveraging the multivariate interactions among multiple brain sources. Decoding surpasses traditional univariate analyses by capturing the complex spatial and temporal patterns of brain activity that correspond to cognitive processes, thereby providing integrative insights into the contributions of each neural source. However, while useful for classifying distinct experimental conditions, decoding does not disentangle the brain processes underlying the measured responses.

In contrast, linear decomposition algorithms are powerful tools in neuroimaging that excel at isolating the brain mechanisms underlying simultaneous cognitive processes by identifying distinct sources of variance in multivariate neural recordings. These approaches have traditionally been applied in numerous studies to derive brain networks from fMRI data, particularly using Principal Component Analysis (PCA) and Independent Component Analysis (ICA)[21-25] (for a recent review see[26]). Although these methods have been successful, they have not been further developed to identify network configurations underlying the perceptual and cognitive processing of external stimuli. This limitation is likely due to the inherent constraints of fMRI, especially its low temporal resolution, which makes it challenging to study brain signal covariance over time in event-related experimental designs[27].

Conversely, the superior temporal resolution of neurophysiological recordings offers great opportunities to study covariance between signals in a relatively short period of time, such as a few seconds, as typically occurs in event-related designs. However, classical studies have predominantly, if not exclusively, used PCA at the topographical scalp level, especially with EEG and, to a lesser extent, MEG. This approach has proven effective for linear reduction of multivariate EEG and MEG data[28-34] (for a review see[35]), facilitating the investigation of event-related potentials/fields (ERPs/ERFs), reducing the dimensionality of electrode/sensor data, and identifying and removing artifacts. However, these studies have not applied these linear decomposition techniques at the neural source level to derive brain networks, missing the full potential that these techniques have to offer. One notable exception is a study that used ICA to derive brain networks from MEG data during resting state[36]. The results revealed network configurations comparable to those often observed in fMRI, providing relevant novel

insights into neurophysiological brain networks. However, the study was limited to resting-state analysis, focusing only on canonical frequency bands. Moreover, it did not provide information on the variance explained by the different networks, nor did it explore network configurations of the brain during external stimulation.

Building on the limitations identified in existing state-of-the-art methods and previous applications of linear decomposition techniques, we have recently developed *Network Estimation via Source Separation* (NESS). NESS is a multivariate framework that employs linear decomposition algorithms to estimate brain networks from source-reconstructed MEG data. Source separation comprises a family of methods aimed at disentangling overlapping cognitive processes generating multivariate neural signals[6]. Crucially, by performing source separation on the entire brain voxel data matrix, NESS directly identifies simultaneous brain networks, returning their explained variance, their spatial configuration for physiological interpretation, and their activation time series for further analysis. In a recent study, we presented the frequency-resolved variant of NESS named *FREQuency-resolved Network Estimation via Source Separation* (FREQ-NESS)[37]. In this variant, generalised eigendecomposition (GED) is utilised to identify and separate brain networks based on their dominant narrow-band activity in continuous recordings. As a result, the decomposition yields comprehensive and physiologically interpretable insights into frequency-specific brain networks underpinning cognitive processes and rest[38-42]. To demonstrate the FREQ-NESS framework, GED was applied to source-reconstructed MEG data within narrow frequency bands (1.2 Hz intervals) during both resting states and continuous periodic auditory stimulation. This application allowed us to distinguish intrinsic frequency-resolved brain networks during resting state and observe their rearrangement in response to continuous auditory stimuli.

In the current work, we build on previous research that used linear decomposition techniques in fMRI resting-state analyses and EEG scalp-level event-related designs to extend the NESS framework by developing BROAD-NESS. This method applies PCA to broadband MEG source-reconstructed brain voxel time series recorded during event-related tasks, with the goal of identifying broadband brain networks that are transiently recruited for different levels of stimulus processing. Specifically, by applying BROAD-NESS to MEG data collected during a musical sequence recognition task, we aim to separate the brain

networks engaged in long-term musical sequence recognition as well as to characterise their spatial configurations and event-related activation time series.

Thus, this study has a twofold objective: (i) advancing our understanding of brain dynamics underlying complex memory functions and (ii) introducing a new tool for investigating brain networks within event-related paradigms.

Results

Overview of the experimental design and MEG source reconstruction

Eighty-three participants engaged in an old/new auditory recognition task during magnetoencephalography (MEG) recordings (**Figure 1a-b**). Following the learning of a brief musical piece (see **Figure S1**), participants were presented with 135 five-tone musical sequences, each lasting 1750 ms. They were asked to indicate whether each sequence belonged to the original music ('memorised' sequence, denoted as M, old) or represented a varied sequence ('novel' sequence, denoted as N, new) (Figure 1a). Among the presented sequences, 27 were directly extracted from the original musical piece, while 108 were variations. These variations were categorised based on the number of musical tones altered following the first tone (NT1), second tone (NT2), third tone (NT3), or fourth tone (NT4) (see **Figure S2**).

After performing the pre-processing of the MEG data (see Methods for details), we computed source reconstruction. We employed a single-shell forward model alongside a beamforming approach as the inverse solution, using an 8-mm grid that corresponded to 3559 brain voxels (**Figure 1c-d**). This procedure produced a time series for each reconstructed brain voxel returning a matrix of 3559 brain voxels x time-points, independently for each participant and experimental condition.

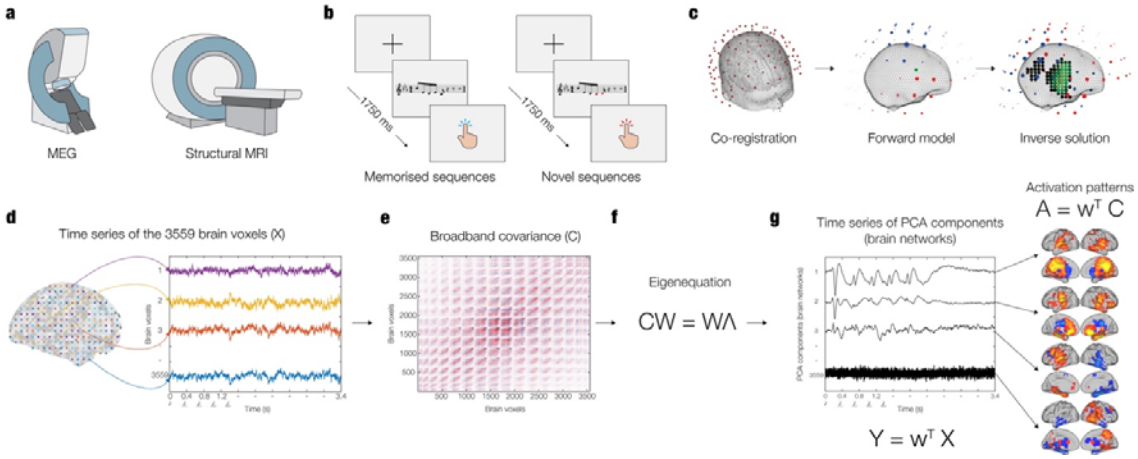

Figure 1: BROADband network estimation via source separation (BROAD-NESS)

The figure provides an overview of the BROAD-NESS methodology. ***a*** *- MEG was used to collect neurophysiological data while participants performed an auditory old/new recognition task.* ***b*** *- Five-tone auditory sequences, presented in random order, were classified by participants as either "old" (memorised*

sequences, M) or "new" (novel sequences, N) using button presses. ***c*** *- Co-registration was performed between MEG data and individual MRI anatomical scans. To reconstruct the neural sources which generated the signal recorded by the MEG, a single shell forward model was used. The inverse solution was estimated through beamforming.* ***d*** *- The source reconstruction yielded time series data for 3559 brain voxels based on an 8-mm grid brain parcellation.* ***e*** *- The covariance matrix (C) was computed from the broadband voxel data matrix. f – Principal Component Analysis (PCA) was computed by solving the eigenequation* $CW = W\Lambda$ *for the eigenvectors (W) to find the weighted combinations of brain voxels to orthogonal components, which reflected brain networks; the associated eigenvalues (*Λ*) express the amount of variance explained by each network component.* ***g*** *- Network activation time series and spatial patterns were derived by applying the spatial filters (W) to the voxel data (X) to obtain network activation time series (Y). The same filters were applied to the covariance matrix to compute the spatial activation patterns (A), representing the components' projections in voxel space.*

PCA, Monte Carlo Simulations (MCS) and statistics

PCA was conducted on the reconstructed time series of the 3559 brain voxels, averaged across participants and conditions, to identify simultaneously operating broadband brain networks (**Figure 1e-f-g**). To assess significant PCA components, a Monte Carlo Simulation (MCS) approach was used by performing PCA on data randomised across the temporal dimension for 100 permutations. Significant principal components from the original data were defined as those explaining more variance than the maximum variance accounted for by the first component across the 100 permutations of the randomised data (see Methods for details). Remarkably, the variance explained by the principal components in the randomised data remained rather consistent across all permutations, suggesting that a conventional set of 100 permutations may not be necessary since a reduced number of permutations (e.g., 50 or even as few as 10) would indeed yield equivalent results.

This procedure identified six significant PCA components, which accounted for the following percentages of variance: 71.75%, 16.32%, 4.16%, 1.30%, 0.99%, 0.92%. Each component was interpreted as a distinct brain network based on its spatial activation pattern, which was obtained by multiplying the component’s eigenvector by the covariance matrix of the data. Unlike FREQ-NESS, which was based on GED, the weights and spatial activation patterns produced by PCA were equivalent in demonstrating the relative contribution of each brain voxel to the network.

As illustrated in **Figure 2**, the first identified brain network comprised the auditory cortices and the medial cingulate gyrus, while the second one included the auditory cortices, anterior cingulate gyrus, ventromedial prefrontal cortex, hippocampal regions, and insula. The remaining four networks were characterised by similar spatial maps; however, they were deemed less relevant as they explained considerably less variance (**Figure S3**).

The weights were subsequently multiplied by the original data to compute the time series for each brain network. It is important to note that while the weights were computed using data averaged across participants and conditions, the computation of the brain network time series was performed independently for each participant and experimental condition. This was necessary to allow statistical comparisons of the brain networks time series across experimental conditions. Specifically, statistical analyses were conducted by contrasting the time series of the memorised versus varied musical sequences, consistent with our prior study focusing on specific brain ROIs. Here, a two-sided t-test was performed for each time point and each combination of memorised versus novel sequences (i.e., M versus NT1, M versus NT2, M versus NT3, M versus NT4). Multiple comparisons were corrected using False Discovery Rate (FDR). This analysis revealed several significant time points where the memorised sequences differed significantly from the novel ones (**Figure 2**).

Detailed statistical results are summarised in **Table S1**.

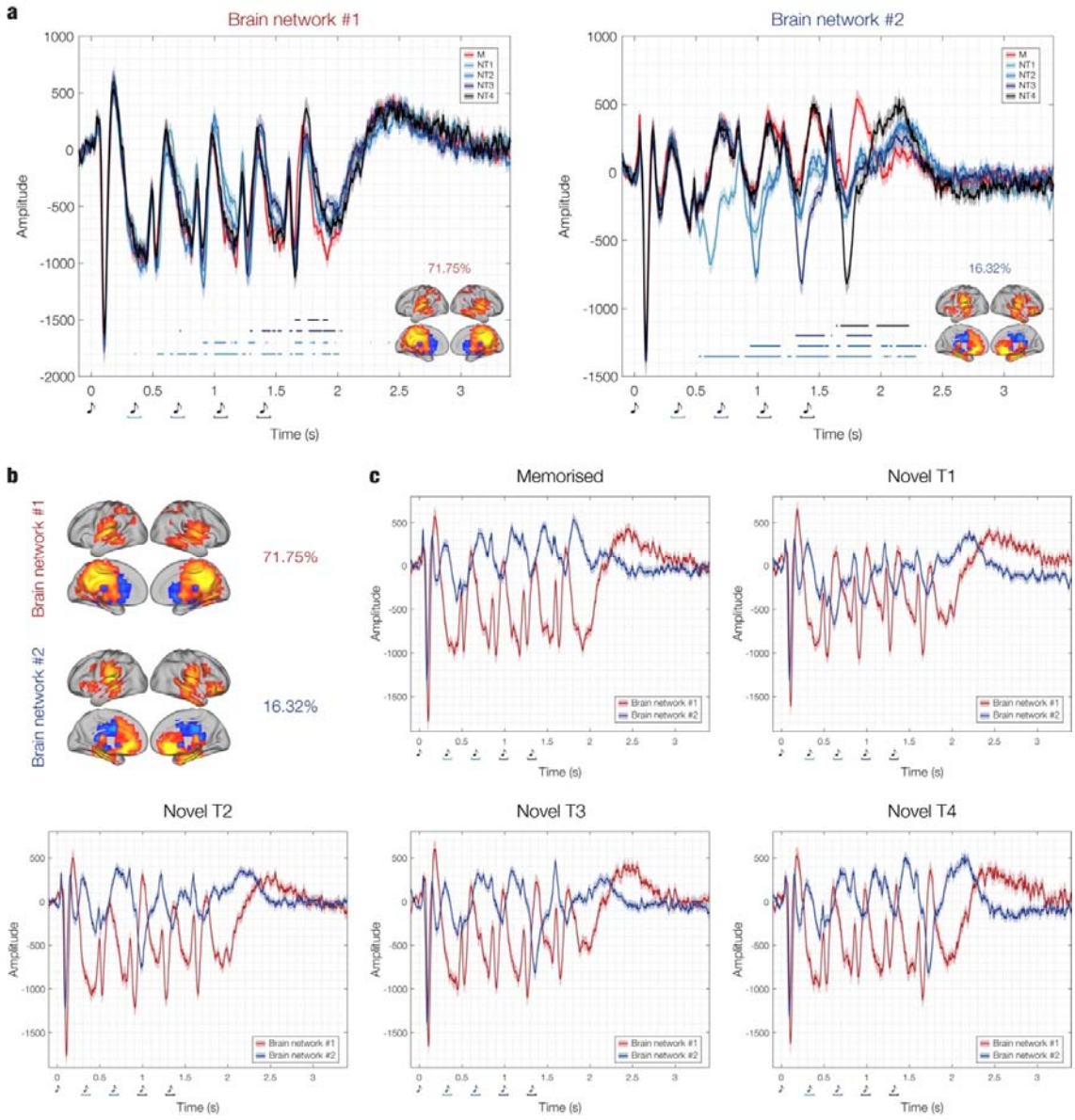

Figure 2: Time series and spatial activation patterns of main brain networks

The figure illustrates the time series and spatial activation patterns of the two brain networks that explained the highest variance (71.75% and 16.32%, respectively). These networks were estimated using PCA within the BROAD-NESS framework, which was computed on the data averaged across conditions and participants. ***a*** *– Independent time series for each participant, brain network, and experimental condition were generated using PCA-derived weights from the averaged data. The individual time series were then averaged across participants, as shown in the plots. Shaded areas represent standard errors. The brain templates illustrate the spatial extent of the networks, with yellow voxels contributing the most and light blue voxels contributing the least to the time series. Only voxels with values exceeding the mean by more than one standard deviation in absolute terms are depicted. Blue-black lines indicate the temporal extent of the significant differences between M versus each category of N (i.e. M versus NT1, M versus NT2, M versus NT3, M versus NT4), computed using*

two-sided t-tests corrected for multiple comparisons via False Discovery Rate (FDR). Different shades of blue-black represent specific M versus N comparisons. ***b*** *- Focus on the spatial activation patterns of the brain networks.* ***c*** *– Focus on the brain networks time series, depicted independently for each experimental condition to emphasise similarities and differences between the two brain networks time series. Musical tone sketches represent the onset of each tone in the sequences.*

Data randomisations and brain networks

In addition to the MCS approach, we aimed to systematically assess how the sensitivity of BROAD-NESS was influenced by the temporal and spatial dimensions of latent brain networks. To achieve this, we independently disrupted the spatial and temporal organisation of the data matrix (brain voxels x time points) by implementing two types of randomizations. The randomisation strategies were designed as follows: (i) space randomisation, where the voxel indices were shuffled row-wise; and (ii) time randomisation, where the time indices were shuffled independently for each brain voxel. As in the case of the Monte Carlo simulations, to evaluate the stability and robustness of the procedure, each randomisation strategy was executed 100 times.

For the first randomisation (space randomisation), we found that the variance explained by the principal components and their associated time series remained identical to those of the original data (**Figure S4**). However, their spatial activation patterns exhibited a completely disrupted structure, indicating that this randomisation did not affect the PCA computation but resulted in non-meaningful spatial extents of the brain networks. In contrast, the second randomisation (time randomisation, which was also used within the MCS approach detailed above) disrupted both the spatial and temporal domains, leading to a significantly reduced variance explained by the main components (**Figure S4**). In this case, the combination of disrupted spatial activation patterns and time series displaying no differences between experimental conditions made the estimated brain networks not interpretable. The same statistical testing described for the original data was performed for both randomisation strategies. The time series and spatial activation patterns obtained from the two randomisation strategies are illustrated in **Figure 3**, while a complete statistical report is provided in **Table S2**.

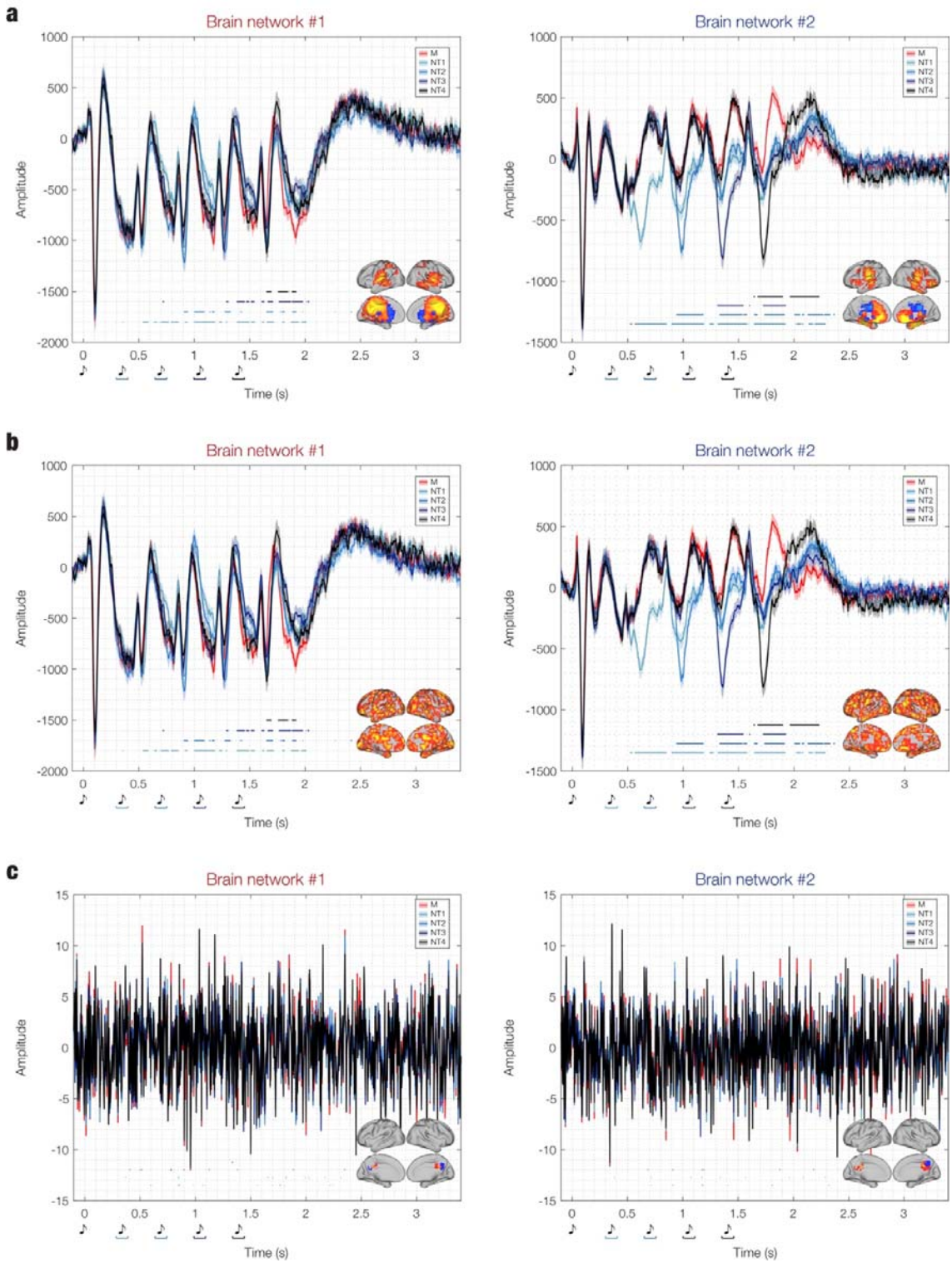

Figure 3: Brain networks estimated from randomised data

This figure illustrates the impact of data randomisation on the estimation of brain networks. ***a*** *- Brain networks computed from the original data, identical to those shown in* ***Figure 2****.* ***b*** *- Space randomisation, where the*

order of the brain voxels was randomised without altering their time series. The time series and explained variance remain the same as in the original data, but the spatial activation patterns are scrambled. This demonstrates that PCA is independent of voxel order, confirming that meaningful patterns in the brain networks are genuine and not artefacts of the PCA algorithm. ***c –*** *Time randomisation, where the time indices of the time series were disrupted, independently for each brain voxel. This leads to meaningless, low-amplitude time series and scrambled activation patterns, mostly concentrated around the mean. As a result, only a few brain voxels are depicted in the templates. In all cases, independent time series for each participant, brain network, and experimental condition were generated using PCA-derived weights from the averaged data. The individual time series were then averaged across participants, as shown in the plots. Shaded areas represent standard errors. The brain templates illustrate the spatial extent of the networks, with yellow voxels contributing the most and light blue voxels contributing the least to the time series. Only voxels with values exceeding the mean by more than one standard deviation in absolute terms are depicted. Blue-black lines indicate the temporal extent of the significant differences between M versus each category of N (i.e. M versus NT1, M versus NT2, M versus NT3, M versus NT4), computed using two-sided t-tests corrected for multiple comparisons via False Discovery Rate (FDR). Different shades of blue-black represent specific M versus N comparisons. The variance explained by the PCA components for the original data and the two randomisation strategies is depicted in* ***Figure S4****.*

Comparing different PCA computations

To enhance the robustness of our analysis and elucidate the subtle differences arising from distinct PCA computation approaches to neural data, we conducted additional analyses. A key question relevant to experimental settings is whether it is more advantageous to compute PCA on individual experimental conditions or on aggregated data (e.g., data averaged over conditions).

In this study, we explored both approaches and compared the results, as illustrated in **Figure S5** and reported in detail in **Table S3**. Specifically, PCA was first computed on the data averaged across conditions, followed by the computation of time series. We also performed PCA independently for each condition, allowing for a direct comparison of the time series derived from the first PCA components and an assessment of the differences. As shown in **Figure 4**, the two computations returned almost identical results, suggesting that the brain networks underlying the different experimental conditions were very similar (yet characterised by different temporal dynamics).

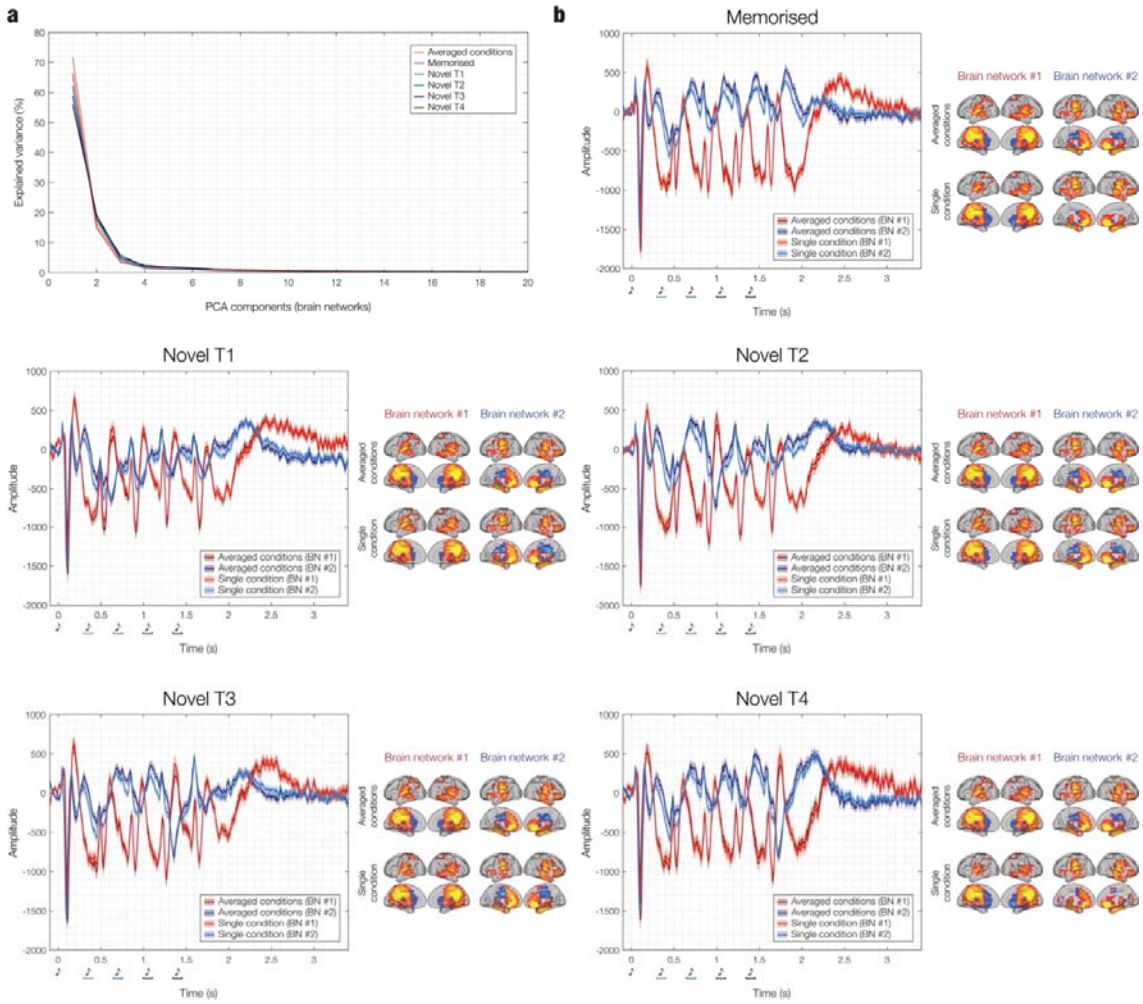

Figure 4: Brain networks estimated from data averaged across conditions or independently for each condition

a *- Variance explained by the PCA components after performing PCA on data averaged across conditions or independently for each condition. The nearly equivalent variance suggests that the different experimental conditions are linked to the same brain networks.* ***b*** *- Comparison of the time series for the two brain networks, computed using PCA weights from either averaged data or data selected independently for each condition. The time series are nearly identical, further supporting the notion that the brain networks underlying the different experimental conditions are extremely similar. Indeed, the differences between experimental conditions arise not in the brain networks spatial extent, but in the polarity and temporal dimension of their responses. In all cases, independent time series for each participant, brain network, and experimental condition were generated using PCA-derived weights from the data averaged across participants. The individual time series were then averaged across participants, as shown in the plots. Shaded areas represent standard errors. The brain templates illustrate the spatial extent of the networks, with yellow voxels contributing the most and light blue voxels contributing the least to the time series. Only voxels with values exceeding the mean by more than one standard deviation in absolute terms are depicted.*

This concept can similarly be applied to the multiple participants involved in the study. PCA can be performed on the average data across participants, followed by the independent reconstruction of time series for each participant using the weights obtained from PCA. Alternatively, PCA can be computed independently for each participant, along with their respective time series, or it can be computed on the concatenated data from all participants and then the time series of each brain network can be reconstructed independently for each participant. We implemented all three approaches and presented a comparison in **Figure 5**, which revealed similar results, with the clearest and most interpretable outcomes obtained from PCA computed on the average data across participants.

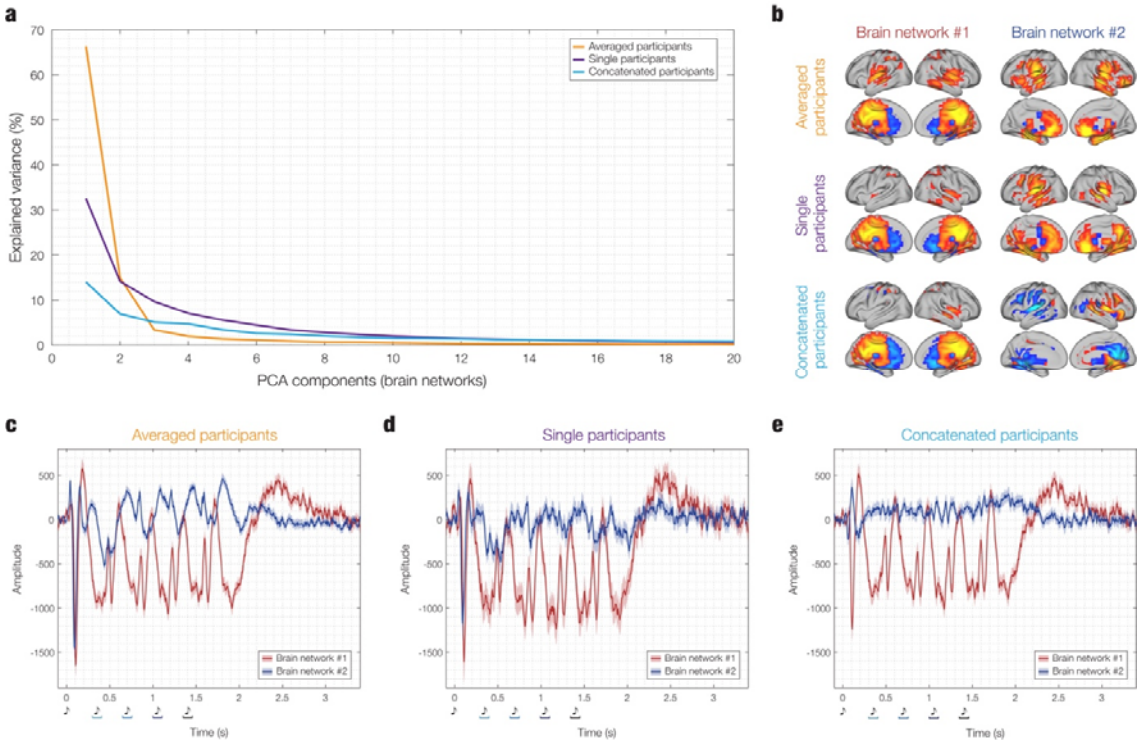

Figure 5: Brain networks estimated from data averaged across participants or independently for each participant

a *- Variance explained by the PCA components after performing PCA on data averaged across participants, or independently for each participant, considering one experimental condition: the previously memorised sequences. The results show a clear reduction in the variance explained by the first components when PCA is performed independently on individual participants (and the results averaged) or on the concatenated data from*

all participants, compared to PCA computed on data averaged across participants. ***b*** *- The spatial activation patterns are depicted in brain templates, with yellow voxels contributing the most and light blue voxels the least to the corresponding time series. Only voxels with values exceeding the mean by more than one standard deviation in absolute terms are depicted. The plots show that the spatial activation patterns of the first brain network remain relatively stable, despite the drop in variance observed in* ***a****. However, the spatial activation patterns for the second brain network show a clear shift. When PCA is computed for individual participants (and results averaged), the network is less clearly defined but still maintains a similar spatial extent. In contrast, when PCA is performed on the concatenated data from all participants, the spatial extent of the second network drastically changes, losing its relevance.* ***c*** *- The time series were generated in three different ways. In the first case, independent time series for each participant and brain network were computed using PCA-derived weights from data averaged across participants. In the second case, PCA was computed independently for each participant, and individual time series were generated using participant-specific PCA weights. In the third case, PCA was computed on the concatenated data from all participants, and those weights were used to independently generate time series for each participant. In all cases, the individual time series were then averaged across participants, as shown in the plots. Shaded areas represent standard errors. Overall, the time series results are consistent with the spatial activation patterns. The first brain network remains relatively stable across the different methods of computation, while the second network shows substantial changes. Specifically, the time series becomes less well-defined in the individual-participant computation and approaches a flat line in the concatenated data computation. This suggests that PCA should be performed on data averaged across participants, and the resulting weights should be used to compute the time series independently for each participant and experimental condition.*

Focus on multiple comparisons corrections

To further enhance the robustness of our results and provide additional insights into the contrasts between brain network time series while correcting for multiple comparisons, we computed and compared three additional correction methods specifically for the contrast between M and N1. The approaches, detailed in the methods section, include: (i) Bonferroni correction, (ii) cluster-based permutation test, and (iii) one-dimensional (1D) cluster-based Monte Carlo Simulation (MCS, α = .05, MCS *p-value* = .001). As illustrated in **Figure S5**, the results were highly convergent, confirming the effectiveness and consistency of all three correction methods.

Discussion

Research in cognitive neuroscience has established that the brain operates as a dynamic system, organised into functionally related networks[43-45]. However, evidence for these networks mostly relies on studies focused on specific brain ROIs, using complex methodologies with numerous assumptions. This approach often limited the potential of the high-dimensional neural data, resulting in fragmented insights and challenges in interpretation.

To address these issues, we developed *BROADband brain Network Estimation via Source Separation* (BROAD-NESS) and applied it to the broadband MEG source reconstructed brain voxels during an event-related auditory recognition task.

BROAD-NESS rests on three key assumptions, each supported by prior evidence: (i) Multivariate time series represent brain voxels as a linear combination of sources mixed with noise, with a brain network forming when independent brain voxels covary over time[23,25,46]; (ii) The PCA components generated by BROAD-NESS are directly interpretable as brain networks[37]; (iii) The variance explained by these components reflects the relative significance of each network, while the associated activation patterns and time series offer insights into their spatial and temporal dynamics[94]. Noteworthy, this variant of NESS is optimised for analysing event-related responses, effectively isolating transient brain networks engaged in different stages of stimulus processing. By leveraging time-locked analyses, BROAD-NESS minimises noise, enabling a clear characterisation of networks that explain a large proportion of the variance in the evoked responses.

Applying BROAD-NESS to MEG data from an auditory recognition task revealed two primary networks, represented by the first two principal components, which together explained 88.06% of the variance (71.75% and 16.31%, respectively). Both components involved the auditory cortices. The first component also included the medial cingulate gyrus, with its time series capturing early auditory processes such as N100 components elicited by each sound, as well as later, slower components remaining active between sounds in the sequence. In addition to auditory cortices, the second component involved hippocampal regions, the inferior temporal cortex, insula, and regions of the prefrontal cortex, including the anterior cingulate and ventromedial prefrontal cortices. Its time series highlighted a slow positive component to each sound, suggesting a process of matching incoming tones to

memory traces of previously heard melodies[47,48]. Additionally, a rapid negative peak was observed in response to variations in the sequence, arguably reflecting prediction errors[49,50].

These positive and negative components align with our previous ROI-based study[7], which similarly found activations and hierarchical relationships between the auditory cortex, cingulate gyri, ventromedial prefrontal cortex, and hippocampus during the same recognition task. In the current study, we move beyond the focus on individual ROIs by identifying two key brain networks involved in the auditory memory task. Both networks engaged the auditory cortices, which were differently connected to either the medial cingulate gyrus or to frontal brain regions and hippocampus. This suggests that the auditory cortex plays a dual role, working with different brain regions to extract sound features and match them to memory traces. These findings, revealed through the multivariate BROAD-NESS approach, offer essential insights that were not achievable with the previous ROI-based analysis.

The findings of the present study also align with previous research. The network identified by the first principal component, involving the auditory cortices and cingulate gyrus, is consistent with previous ROI-based studies on functional and structural connectivity, which have demonstrated strong links between these regions in both humans and animals[51-53]. This suggests their joint involvement in a network responsible for early auditory processing and sustained attention to the auditory sequence[54-56]. Similarly, the network identified by the second principal component activated regions typically associated with memory and predictive functions[57-59]. Previous studies have also reported the combined activation of memory-related brain regions in both structural and functional connectivity, supporting their role in generating and evaluating predictions by comparing incoming sounds with stored memory traces[60].

The MCS approach described in the current study also identified four additional networks, each explaining a relatively small percentage of the variance (4.16%, 1.30%, 0.99% and 0.92%, respectively). These networks included subsets of regions from the first two principal components but were characterised by less interpretable time series activation patterns, likely reflecting residual activity not captured by the main components, mixed with noise. Given their lower explained variance, the relevance of these networks is negligible compared to the first two.

In its essence, BROAD-NESS presents three key advantages over previous approaches to network estimation and event-related responses. First, it does not rely on predefined ROIs, as

it operates on the entire source-reconstructed MEG space. This comprehensive approach, applied to the 3559-voxel grid with 8 mm resolution, is considered optimal for balancing spatial detail with the actual resolution of MEG data. By avoiding the reduction of data to predefined ROIs, as in traditional methods (e.g.[61-63]), BROAD-NESS preserves crucial spatial information, fully leveraging the benefits of MEG source reconstruction. Unlike ROI-based approaches that require a priori selection of brain regions, BROAD-NESS analyses all available data in voxel space, allowing for a data-driven exploration of brain activity.

Second, BROAD-NESS presents significant advantages in terms of simplicity and efficiency. It relies on a few well-supported assumptions, leading to results that are straightforward to interpret. The mathematical foundations of BROAD-NESS, which include covariance and eigenvector solutions—key elements of PCA — are relatively simple and less susceptible to artifacts compared to more complex signal processing techniques. Additionally, BROAD-NESS is extremely fast to compute, making it highly efficient for a variety of event-related paradigms, even with limited computational power or for large datasets. These unique features distinguish BROAD-NESS from other methods with similar aims and facilitate its integration with existing approaches. For instance, (i) BROAD-NESS can be effectively integrated with existing methods typically applied to brain ROIs to investigate non-linearity in the brain. While BROAD-NESS does not directly assess non-linear relationships, it disentangles simultaneous brain networks, which can then be examined for non-linearity using techniques such as TE and DCM. These methods can be applied to the time series generated by BROAD-NESS, allowing for the exploration of non-linear interactions between entire brain networks rather than isolated ROIs. Furthermore, BROAD-NESS typically identifies a few large brain networks by focusing on a small number of principal components that explain most of the variance in the data. In this study, for instance, we identified two key networks accounting for 88% of the total variance. This streamlined approach not only reduces the computational demands for analyses like TE and DCM by retaining only the key data but also addresses the common challenge of defining ROIs, which often leads to excluding valuable data. Importantly, (ii) BROAD-NESS does not assume recurrent states in brain activity, in contrast to approaches like HMMs and LEiDA. However, while recurrent states are not the primary focus here, they can still be inferred through multivariate recurrence analysis of the time series generated by BROAD-NESS[64,65]. Similarly, (iii) while BROAD-NESS does not directly infer directionality or causality

between brain networks, it provides time series data that can be further analysed using existing methods designed for such purposes, like GC or TE. In summary, while BROAD-NESS does not provide direct information regarding non-linearity, recurrent states, or directionality, it offers essential insights without assumptions about the spatial extent of the brain networks involved, paving the way for further examination of these metrics directly at a network level.

Third, BROAD-NESS effectively applies PCA to MEG source-reconstructed data in event-related designs to derive brain networks. Remarkably, BROAD-NESS retains both temporal resolution — similar to previous EEG studies computing dimensionality reduction at the scalp-level with PCA[66-71] (for a review see[72]) — and, to a reasonable extent, spatial resolution, comparable to fMRI studies that applied ICA and PCA at the brain voxel level[21,22,24,25,73-75] to derive resting state brain networks over long recordings. The implementation of PCA in BROAD-NESS addresses limitations inherent to both methods, namely the limited interpretability of MEEG sensors and the slower temporal dynamics of fMRI. By achieving an optimal trade-off between temporal and spatial resolution, our approach enables the identification of transient, rapid networks recruited for specific functions related to stimulus processing, while maintaining physiological interpretability.

Lastly, a few technical considerations warrant attention when applying PCA across multiple participants. In our study, we compared outputs from PCA applied to data averaged across all participants with PCA computed independently for each participant, followed by averaging the outputs, and with PCA applied to concatenated participant data. Although these approaches yielded coherent results, they differed significantly in clarity. PCA on averaged data produced cleaner and more interpretable results, exhibiting a sharper exponential decline in the variance explained by each principal component. In contrast, PCA on single participants and on concatenated data revealed potentially nuanced but less distinct patterns. Essentially, this discrepancy can be interpreted in two ways: (i) PCA applied to individual participants (either single participants or concatenated data) may capture more detailed information regarding inter-individual differences in brain networks, suggesting that the additional information retained is relevant to brain processes; or (ii) PCA on individual participants is simply decomposing a noisier matrix, resulting in less refined patterns and obscuring the clarity of the actual brain information. While we cannot conclusively determine which interpretation is correct, the tests conducted in this study, alongside previous

recommendations for event-related designs in neurophysiology[76] favour averaging across participants before computing PCA. This approach effectively reduces noise from both environmental factors and individual variability, thereby enhancing generalisability across the population. Notably, this approach contrasts with the strategy employed in FREQ-NESS, where GED is computed independently for each participant using continuous data without averaging. This is essential to maintain the frequency-resolved content of the signal, which would otherwise be suppressed by averaging[37]. In contrast, BROAD-NESS focuses on broadband networks and leverages time-locked averaging to maximise the signal-to-noise ratio of event-related brain activation, resulting in considerably higher variance explained by the relevant networks.

To further explore the effects of averaging on our analysis, we applied PCA to either the data averaged across experimental conditions or to each condition separately. The results from these two approaches were nearly overlapping, indicating that the different conditions engaged almost identical brain networks. Importantly, computing PCA on the averaged data allowed us to properly derive the time series for the different conditions, enabling correct statistical testing. However, this approach is only valid if the experimental conditions activate similar brain networks; if they instead recruit significantly different networks, averaging is not appropriate. Thus, no definitive recommendation can be made, and the choice between these two alternative solutions should depend on the specific experimental protocol and hypotheses.

Finally, randomising the order of brain voxels, as observed in the evaluation of FREQ-NESS[37], did not impact the variance explained or the resulting brain networks time series in this study; however, it did alter the spatial activation patterns. In contrast, randomising the data order over time disrupted the relationships within the data, resulting in significant reduction of the slope of the exponential decay of the variance explained by the principal components. It did also disrupt the clarity of the brain networks time series and the spatial activation patterns, further demonstrating the effectiveness of BROAD-NESS on real neural data.

In conclusion, this study described the BROAD-NESS method, establishing a strong foundation for applying it to a diverse range of event-related datasets. Expanding its use to explore various sensory domains and cognitive processes could provide valuable insights into the brain networks underlying these events. Future research should focus on systematically

comparing BROAD-NESS with traditional ROI-based methods to determine whether the networks observed are merely a summation of ROI activations or if they reveal higher-order interactions, as suggested by the current findings. Such comparisons could elucidate whether the networks identified by BROAD-NESS reflect more complex neural dynamics that extend beyond the capabilities of the single brain ROIs. Additionally, as previously mentioned, BROAD-NESS is well-suited for integration with existing methods to examine directionality, recurrence, and non-linear interactions among brain networks, all solutions that should be explored by future research. Finally, significant advancements within the NESS framework can also be made by investigating induced responses in event-related designs, enhancing our understanding of oscillatory brain behaviour and providing deeper insights into the temporal dynamics of cognition and its underlying neural mechanisms.

Methods

Participants

The participant sample comprised 83 volunteers [33 males and 50 females (biological sex, self-reported)] aged between 19 and 63 years (mean age: 28.76 ± 8.06 years). Participants were recruited in Denmark, primarily from Western countries. Information on gender was not collected, as it fell outside the scope of this research. All participants were healthy, reported normal hearing, and had relatively homogeneous educational backgrounds. Specifically, 73 participants either held a university degree (bachelor's or master's, n = 54) or were currently enrolled as university students (n = 19). Of the remaining 10 participants, five held a professional degree earned after high school, and the other five had only completed high school. The study was approved by the Institutional Review Board (IRB) of Aarhus University (case number: DNC-IRB-2020-006) and conducted in accordance with the Declaration of Helsinki – Ethical Principles for Medical Research. All participants provided informed consent prior to the experiment and received compensation for their participation.

Experimental stimuli and design

In this study, we employed an old/new auditory recognition task during magnetoencephalography (MEG) recordings (**Figure 1**), as described in previous studies[7,96,97,98,99,100]. Participants first listened to a short musical piece twice and were asked to memorise it. The piece consisted of the first four bars of the right-hand part of Johann Sebastian Bach's Prelude No. 2 in C Minor, BWV 847, where each bar contained 16 tones, totalling 64 tones. Each tone lasted approximately 350 ms, making the total duration 22,400 ms. A final tone, lasting 1000 ms, was added for a sense of closure, bringing the full duration to 23,400 ms (23.4 seconds). The musical notation for the prelude is shown in **Figure S1**.

After memorising the piece, participants were presented with 135 five-tone musical excerpts, each lasting 1750 ms. They were asked to determine whether each excerpt belonged to the original music ('memorised' sequence [M], old) or was a variation ('novel' sequence [N], new). Among the excerpts, 27 were taken directly from the original musical piece, while the remaining 108 were variations. **Figure S2** provides a visual representation of all the sequences used in the study.

The memorised sequences (M) were composed of the first five tones from the first three measures of the original piece, and each sequence was repeated nine times, totalling 27 trials. Novel sequences (N) were created by systematically varying the M sequences. For each of the three M sequences, nine variations were created by altering tones after the first (NT1), second (NT2), third (NT3), or fourth (NT4) tone, resulting in 27 variations per category and 108 novel sequences overall.

The variations followed several strategies. In some cases, the melodic contour was inverted, reversing the melodic direction of the original sequence. In other instances, the remaining tones were scrambled, or the same tone was repeated multiple times, sometimes varying only the octave. Another approach scrambled the intervals between tones. In most cases, the harmonic structure of the novel sequences was preserved relative to the original sequence. Further information about the sequences is reported in Bonetti et al.[7].

This procedure allowed us to explore the brain networks dynamics involved in recognising previously memorised auditory sequences and in the conscious detection of sequence variations. The musical piece and sequences described above were generated as MIDI versions using Finale (version 26, MakeMusic, Boulder, CO) and presented through Psychopy v3.0.

Data acquisition

The MEG recordings were conducted in a magnetically shielded room at Aarhus University Hospital (AUH), Denmark, using an Elekta Neuromag TRIUX MEG scanner with 306 channels (Elekta Neuromag, Helsinki, Finland). Data was collected at a sampling rate of 1000 Hz with an analogue filtering of 0.1 - 330 Hz. Prior to the recordings, participants' head shapes and the positions of four Head Position Indicator (HPI) coils were registered relative to three anatomical landmarks using a 3D digitizer (Polhemus Fastrak, Colchester, VT, USA). This information was later used to co-register the MEG data with anatomical MRI scans. Throughout the MEG recording, the HPI coils continuously tracked the position of the head, allowing for movement correction during analysis. Additionally, two sets of bipolar electrodes were used to monitor cardiac rhythm and eye movements, facilitating the removal of electrocardiography (ECG) and electrooculography (EOG) artefacts in the analysis phase.

MRI scans were obtained on a CE-approved 3T Siemens MRI scanner at AUH. The data included structural T1 (mprage with fat saturation) scans, with a spatial resolution of 1.0 x 1.0

x 1.0 mm and the following sequence parameters: echo time (TE) of 2.61 ms, repetition time (TR) of 2300 ms, a reconstructed matrix size of 256 x 256, an echo spacing of 7.6 ms, and a bandwidth of 290 Hz/Px.

The MEG and MRI recordings were conducted on separate days.

MEG data pre-processing

The raw MEG sensor data (comprising 204 planar gradiometers and 102 magnetometers) was initially pre-processed using MaxFilter[77] (version 2.2.15) to reduce external interferences. We applied signal space separation (SSS) with the following MaxFilter parameters: downsampling from 1000 Hz to 250 Hz, movement compensation via continuous HPI coils (default step size: 10 ms), and a correlation limit of 0.98 to reject overlapping signals between inner and outer subspaces during spatiotemporal SSS.

The MEG data was converted into Statistical Parametric Mapping (SPM) format and further processed and analysed using MATLAB (MathWorks, Natick, MA, USA), incorporating custom-built scripts (LBPD, https://github.com/leonardob92/LBPD-1.0.git) and the Oxford Centre for Human Brain Activity (OHBA) Software Library (OSL)[78] (https://ohba-analysis.github.io/osl-docs/), which integrates Fieldtrip[79], FSL[80], and SPM[81] toolboxes.

Next, the continuous MEG data underwent visual inspection via the OSLview tool to remove any large artifacts, though less than 0.1% of the collected data was discarded. Independent Component Analysis (ICA) was then used (with OSL implementation) to eliminate eyeblink and heartbeat artifacts[82]. The ICA process involved decomposes the original signal into independent components and correlating them with the activity recorded by the electrooculography (EOG) and electrocardiography (ECG) channels[83]. Components that showed a correlation at least three times higher than others were flagged as reflecting EOG or ECG activity. These flagged components were further validated through visual inspection, ensuring their topographic distribution matched typical eyeblink or heartbeat activity, and were subsequently discarded. The signal was then reconstructed using the remaining components.

Finally, the data was segmented into 135 trials (27 M, 27 NT1, 27 NT2, 27 NT3, and 27 NT4) and baseline-corrected by subtracting the mean baseline signal from the post-stimulus data. Each trial lasted 4500 ms (4400 ms of data and 100 ms of baseline).

Source reconstruction

MEG is a powerful tool for detecting whole-brain activity with excellent temporal resolution. However, to fully understand the brain activity involved in complex cognitive tasks, it is essential to identify the spatial sources of this activity. This requires solving the inverse problem, as the MEG recordings reflect neural signals from outside the head but do not directly indicate which brain regions generated them. To address this, we employed beamforming algorithms[84,86,88], using a combination of in-house-developed codes alongside the OSL, SPM, and FieldTrip toolboxes. The procedure consisted of two main steps: (i) designing a forward model and (ii) computing the inverse solution.

First, a single-shell forward model was constructed using an 8-mm grid. This head model treats each brain source as an active dipole and describes how the activity of such a dipole would be detected across MEG sensors[84,85]. The MEG data was co-registered with individual MRI T1-weighted images, using the 3D digitizer information to align the data. When individual anatomical scans were unavailable, an MNI152-T1 template with 8-mm spatial resolution was used to compute the forward model.

Second, a beamforming algorithm was applied as the inverse model. Beamforming uses a set of weights applied to different source locations (dipoles) to isolate the contribution of each brain source to the activity recorded by the MEG sensors[86-88]. This was done for every time point of the recorded brain data, allowing us to reconstruct the spatial sources of the MEG signal. The detailed steps for implementing the beamforming algorithm are provided below.

The data recorded by the MEG sensors (*B*) at time *t*, can be described by the following Eq. (1):

$$B_{(t)} = L * Q_{(t)} + \varepsilon \qquad (1)$$

where *L* is the leadfield model, *Q* is the dipole matrix carrying the activity of each active dipole (*q*) at time *t*, and is noise (for details, see Huang et al.[84]) To solve the inverse problem, *Q* must be estimated for each *q*. In the beamforming algorithm, a series of weights are computed to describe the transition from MEG sensors to the active dipole *q*, independently for each time point. This is reported in Eq. (2):

$$q_{(t)} = W^T * B_{(t)} \quad (2)$$

Here, the superscript T refers to transpose matrix. To compute the weights (W), matrix multiplication between L and the covariance matrix of MEG sensors (C) is performed. Importantly, the covariance matrix C was computed on the signal after concatenating the single trials of all experimental conditions. For each dipole q, the weights (W_q) were computed as shown in Eq. (3):

$$W_{(q)} = (L_{(q)}{}^T * C^{-1} * L_{(q)})^{-1} * L_{(q)}{}^T * C^{-1} \quad (3)$$

The computation of the leadfield model L was performed for the three main orientations of each dipole [85]. Before computing the weights, to simplify the beamforming output[89,90], the orientations were reduced to one using the singular value decomposition algorithm on the matrix multiplication reported in Eq. (4):

$$L = svd(l^T * C^{-1} * l)^{-1} \quad (4)$$

Here, l represents the leadfield model with the three orientations, while L is the resolved one-orientation model that was utilized in Eq. (3).

Once computed, the weights were normalised for counterbalancing the reconstruction bias towards the center of the head [86,91-93] and applied to the neural activity averaged over trials, independently for each time point (Eq. 2) and experimental condition. This procedure returned a time series for each of the 3559 brain sources[86,92].

Principal Component Analysis (PCA), Monte-Carlo simulations (MCS) and randomisations

PCA was applied to the 3559 reconstructed brain sources time series to disentangle broadband brain networks operating simultaneously. PCA is a dimensionality reduction method that transforms data into new variables, or principal components, which account for the most variance within the dataset. This is achieved by computing the eigenvectors and eigenvalues of the data's covariance matrix and then projecting the data onto the directions of maximum variance. Traditionally, PCA simplifies high-dimensional data while retaining the most important information.

In this study, however, PCA was applied to a dense set of MEG-reconstructed brain data at the voxel level (3559 brain voxel time series). The goal was not just to reduce the dimensionality but to identify brain networks (corresponding to the PCA components) through the application of PCA on the 3559 brain voxel time series.

In short, PCA operates as follows: First, the data is centred by subtracting the mean of each brain voxel timeseries from the dataset *X*, as represented by Eq. (5):

$$\bar{X} = X - \mu \tag{5}$$

where μ is the mean vector of *X*.

Then, the covariance matrix *C* is computed on the centred data, as shown in Eq. (6):

$$C = \frac{1}{n-1} \bar{X}^T \bar{X} \tag{6}$$

where *n* is the number of data points.

Then the eigenvalue equation for the covariance matrix is solved to find eigenvalues and eigenvectors, Eq. (7):

$$CW = W\Lambda \tag{7}$$

Where W is the eigenvector matrix (set of weights for each principal component) and Λ is the diagonal matrix of the corresponding eigenvalues (which indicate the amount of variance explained by each component).

Then, the eigenvectors w were used to compute the activation time series of each brain network *Y* by multiplying them by the original data *X*, as shown in Eq. (8):

$$\mathrm{Y} = w^T \mathrm{X} \tag{8}$$

Furthermore, we computed the spatial projection of the components (spatial activation patterns *A*) in brain voxel space. This was done by multiplying the weights of the analysis (the eigenvectors w in this case) by the covariance matrix *C*, as shown in Eq. (9):

$$A = w^T C \quad (9)$$

Interestingly, while previous studies on interpreting weights from multivariate analyses in MEG data have recommended calculating spatial activation patterns[94], in this case, the relative contribution of each brain voxel to the network remains the same, whether using the direct eigenvector w or computing the spatial activation patterns.

Importantly, as detailed in the following section, the PCA procedure was applied across various scenarios to ensure a comprehensive evaluation of the algorithm's performance. This included performing PCA independently for each participant and condition, as well as on data averaged across participants and conditions.

Finally, we aimed to systematically assess how the sensitivity of BROAD-NESS was influenced by the temporal and spatial dimensions of latent brain networks. To achieve this, we independently disrupted the spatial and temporal organisation of the data matrix (brain voxels x time points) by implementing two types of randomizations. The randomisation strategies were designed as follows: (i) space randomisation, where the voxel indices were shuffled row-wise; and (ii) time randomisation, where the time indices were shuffled independently for each brain voxel. To evaluate the stability and robustness of the procedure, each randomisation strategy was executed 100 times. The same statistical testing described for the original data was also performed for both randomisation strategies.

Additionally, the second randomisation was employed in a Monte Carlo simulation (MCS) solution. In this case, we retained the variance explained by the first component of the PCA computed on the randomised data for each of the 100 permutations. This produced a reference distribution of the variance explained by the first component in the randomised data. This reference distribution was then compared to the variance explained by the components in the original data, which were deemed significant only if they explained a greater variance than the highest explained variance in the reference distribution.

Time series and spatial activation patterns of the brain networks that were significant following the MCS approach are illustrated in **Figures 2** and **S3**, while the selective effects of each randomisation strategy are presented in **Figures 3** and **S4**.

Comparing different PCA computations

To enhance the robustness of our work and provide greater insight into the subtle differences associated with the computation of PCA on neural data, we examined a crucial aspect relevant to experimental settings. Specifically, when multiple experimental conditions are present, it is essential to determine whether it is more beneficial to compute PCA on individual conditions or on aggregated conditions (e.g., data averaged over conditions).

To address this, we computed both approaches and compared the results, as illustrated in **Figure 4**. Specifically, we first conducted PCA on the data averaged across conditions and then reconstructed the time series. Subsequently, we computed PCA independently for each condition. This allowed us to compare the brain networks time series of the conditions computed in the two approaches and assess any difference.

A similar consideration applies to the multiple participants in our study, where we explored three possible approaches for computing PCA. The first approach involved performing PCA on the average across participants, followed by reconstructing the time series independently for each participant using the weights obtained from this analysis. The second approach entailed performing PCA independently for each participant along with their respective time series. Finally, the third approach consisted of computing PCA on the concatenated data from all participants, and then deriving the time series independently for each participant.

We implemented all three approaches and compared the results, as illustrated in **Figure 5**.

Statistical analysis

After computing PCA and the time series of the brain networks for each participant and experimental condition, we conducted statistical analyses by contrasting the time series of the previously memorised versus the varied melodies. This approach was consistent with our earlier study that focused solely on brain ROIs[7]. Specifically, we performed a two-sided t-test for each time point across all combinations of M versus N melodies (i.e., M versus NT1, M versus NT2, M versus NT3, M versus NT4). Subsequently, we applied False Discovery Rate (FDR) corrections to account for multiple comparisons.

To strengthen the robustness of our findings and offer deeper insights into the process of contrasting time series of brain networks, we implemented and compared three alternative

methods for correcting for multiple comparisons. This analysis specifically focused on the contrast between M versus NT1, as illustrated in **Figure S5**.

First, we applied the Bonferroni correction, which is a stringent method that adjusts the significance level (α = .05) by dividing it by the number of tests performed, thereby reducing the likelihood of false positives.

Second, we used a cluster-based permutation test, as described by Maris and Oostenveld[95]. Initially, we conducted statistical tests on the original data, as described earlier. We then identified clusters of neighbouring significant time points by applying a threshold to the statistical results (α = .05). Next, we performed 1000 permutations, where, for each permutation, the labels of the two experimental conditions were shuffled for each participant, and the statistics were recalculated. For each permutation, we computed the maximum cluster size of the significant time points, mirroring the approach used for the original data. This yielded a reference distribution of significant clusters, which we compared with the clusters from the original data. Clusters in the original data were deemed significant only if their sizes exceeded the maximum cluster size observed in the permuted data at least 99.9% of the time.

Third, we conducted a one-dimensional (1D) cluster-based MCS (MCS, α = .05, MCS p-value = .001), as detailed in our previous studies[7,96-102]. This approach involved identifying clusters of significant neighbouring time points obtained from the t-tests described above and then performing 1000 permutations to randomise these significant values. For each permutation, we extracted the maximum cluster size to establish a reference distribution. The original clusters were considered significant if they were larger than 99.9% of the clusters obtained from the permuted statistical results. This method is similar to the cluster-based permutation test but should be regarded as an empirical approach. Its primary advantage lies in its computational efficiency, delivering results much faster than the permutation test as it does not require recalculating statistics. Instead, it works directly with clusters formed from the statistics computed on the original data. However, a limitation is that this empirical method does not adhere to classical inferential statistical principles. In our analysis, we clarify how this approach relates to the permutation test, highlighting their respective advantages and limitations in the context of statistical testing for brain data time series.

Data availability

The pre-processed neuroimaging data generated in this study have been deposited in the Zenodo database under accession code [https://doi.org/10.5281/zenodo.10715160][103] and are publicly available. The raw neuroimaging data are protected and are not available due to data privacy laws.

Code availability

The MEG data was first pre-processed using MaxFilter 2.2.15. Then, the data was further pre-processed using Matlab R2016a or later (MathWorks, Natick, Massachusetts, United States of America). Specifically, we used codes from the Oxford Centre for Human Brain Activity Software Library (OSL), FMRIB Software Library (FSL) 6.0, SPM12 and Fieldtrip.

In-house-built code and functions used in this study are part of the LBPD repository which is available at the following link: https://github.com/leonardob92/LBPD-1.0.git

The full analysis pipeline used in this study is available at the following link: https://github.com/leonardob92/BROADNESS_MEG_AuditoryRecognition.git

Acknowledgements

The Center for Music in the Brain (MIB) is funded by the Danish National Research Foundation (project number DNRF117).

L.B. is supported by Lundbeck Foundation (Talent Prize 2022), Carlsberg Foundation (CF20-0239), Center for Music in the Brain, Linacre College of the University of Oxford (Lucy Halsall fund) and Nordic Mensa Fund.

M.L.K. is supported by Center for Music in the Brain and Centre for Eudaimonia and Human Flourishing, which is funded by the Pettit and Carlsberg Foundations.

In addition, we thank the Department of Physics of the University of Bologna for the support provided to C.M., Fundación Mutua Madrileña (Mutua Madrileña Foundation, Madrid, Spain) for the support provided to G.F.R. and Mensa: The International High IQ Society (Italian section) for the support provided to F.C.

Author contributions statement

L.B., G.F.R., M.H.A. and M.R. conceived the hypotheses. L.B. designed the study. L.B., M.L.K. and P.V. recruited the resources for the experiment. L.B., G.F.R. and F.C. collected the data. L.B., G.F.R., M.H.A., C.M. and M.R. performed pre-processing, statistical analysis and linear decomposition of the neural signal. L.B., C.M., M.H.A. and M.R. developed the code for the BROAD-NESS framework. M.L.K., C.T., P.V. and M.R. provided essential help to interpret and frame the results within the neuroscientific and analytical literature. M.H.A. and L.B. wrote the first draft of the manuscript, which was primarily integrated by M.R. and G.F.R. The figures were prepared by L.B., G.F.R. and C.M. All the authors contributed to and approved the final version of the manuscript.

Competing interests statement

The authors declare no competing interests.

SUPPLEMENTARY MATERIAL

Supplementary materials related to this study are organised as supplementary figures (*i*) and tables (*ii*).

Supplementary figures

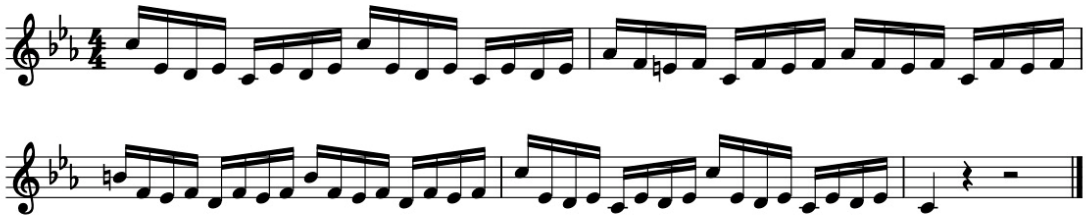

Figure S1. Musical piece used during the encoding phase of the auditory old/new paradigm *In the initial stage of the auditory old/new paradigm, participants listened to a brief musical piece twice and were instructed to memorise it as thoroughly as possible. The piece comprised the first four bars of the right-hand section of Johann Sebastian Bach's Prelude No. 2 in C Minor, BWV 847. Each bar contained 16 notes, resulting in a total of 16 x 4 = 64 notes. Each note lasted approximately 350 ms, amounting to a total duration of 22,400 ms. Additionally, to create a sense of musical closure, we included a final note after the four bars that lasted 1,000 ms. Consequently, the total duration was 23,400 ms, which equals 23.4 seconds. This figure presents the piece in musical notation.*

Melody 1

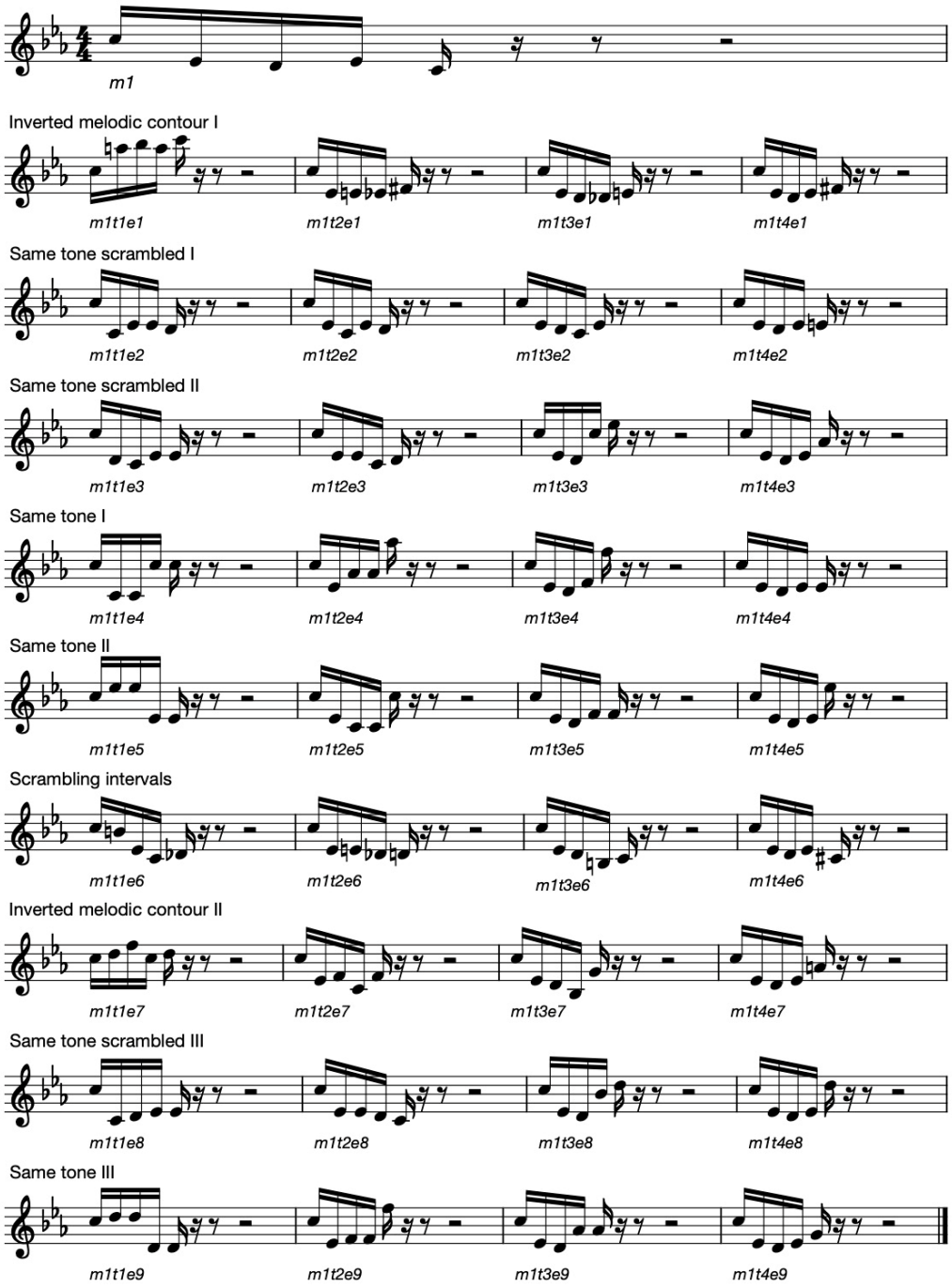
m1
Inverted melodic contour I
m1t1e1
m1t2e1
m1t3e1
m1t4e1
Same tone scrambled I
m1t1e2
m1t2e2
m1t3e2
m1t4e2
Same tone scrambled II
m1t1e3
m1t2e3
m1t3e3
m1t4e3
Same tone I
m1t1e4
m1t2e4
m1t3e4
m1t4e4
Same tone II
m1t1e5
m1t2e5
m1t3e5
m1t4e5
Scrambling intervals
m1t1e6
m1t2e6
m1t3e6
m1t4e6
Inverted melodic contour II
m1t1e7
m1t2e7
m1t3e7
m1t4e7
Same tone scrambled III
m1t1e8
m1t2e8
m1t3e8
m1t4e8
Same tone III
m1t1e9
m1t2e9
m1t3e9
m1t4e9

891

Melody 2

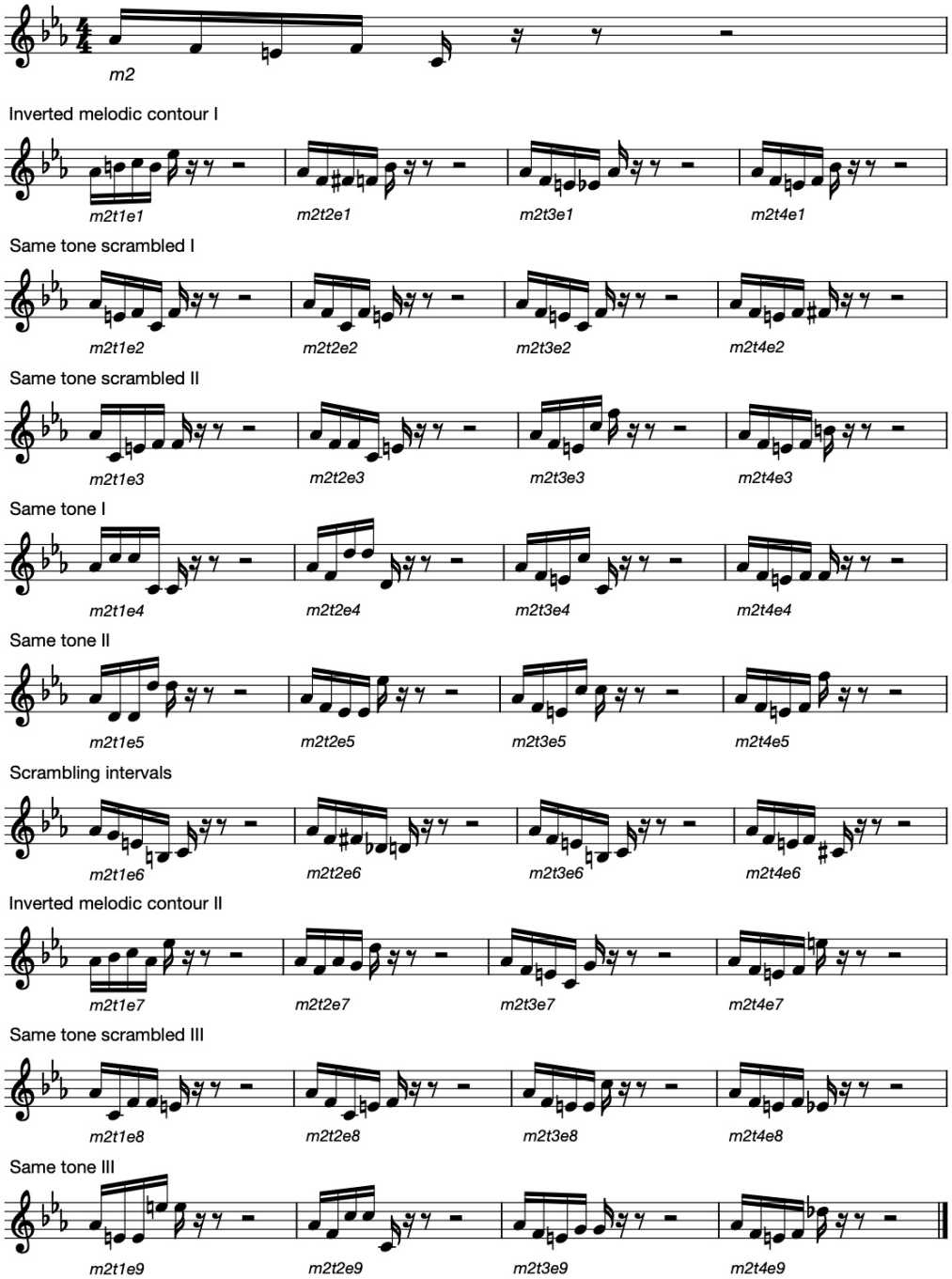
m2
Inverted melodic contour I
m2t1e1
m2t2e1
m2t3e1
m2t4e1
Same tone scrambled I
m2t1e2
m2t2e2
m2t3e2
m2t4e2
Same tone scrambled II
m2t1e3
m2t2e3
m2t3e3
m2t4e3
Same tone I
m2t1e4
m2t2e4
m2t3e4
m2t4e4
Same tone II
m2t1e5
m2t2e5
m2t3e5
m2t4e5
Scrambling intervals
m2t1e6
m2t2e6
m2t3e6
m2t4e6
Inverted melodic contour II
m2t1e7
m2t2e7
m2t3e7
m2t4e7
Same tone scrambled III
m2t1e8
m2t2e8
m2t3e8
m2t4e8
Same tone III
m2t1e9
m2t2e9
m2t3e9
m2t4e9

892

Melody 3

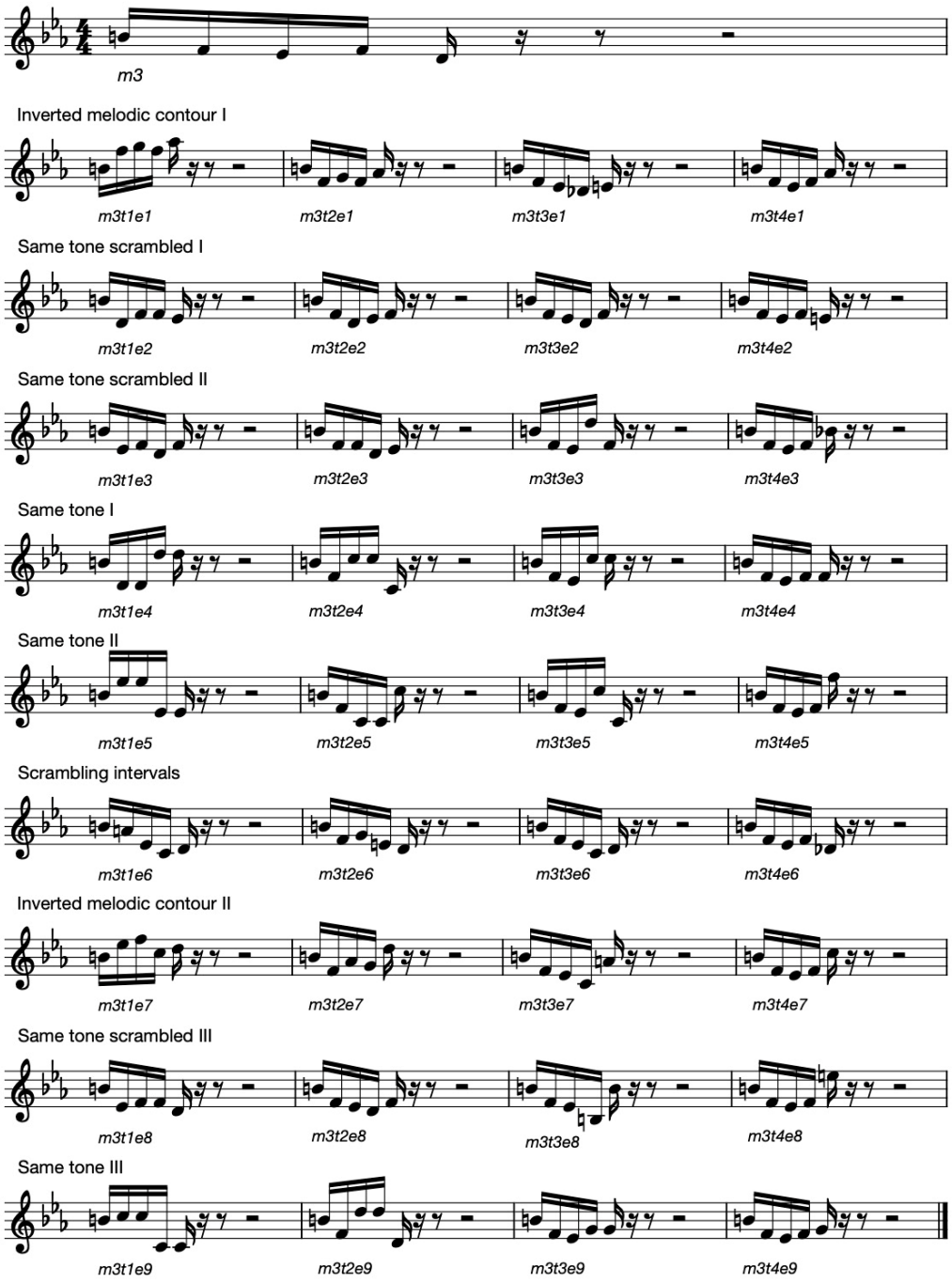
m3
Inverted melodic contour I
m3t1e1
m3t2e1
m3t3e1
m3t4e1
Same tone scrambled I
m3t1e2
m3t2e2
m3t3e2
m3t4e2
Same tone scrambled II
m3t1e3
m3t2e3
m3t3e3
m3t4e3
Same tone I
m3t1e4
m3t2e4
m3t3e4
m3t4e4
Same tone II
m3t1e5
m3t2e5
m3t3e5
m3t4e5
Scrambling intervals
m3t1e6
m3t2e6
m3t3e6
m3t4e6
Inverted melodic contour II
m3t1e7
m3t2e7
m3t3e7
m3t4e7
Same tone scrambled III
m3t1e8
m3t2e8
m3t3e8
m3t4e8
Same tone III
m3t1e9
m3t2e9
m3t3e9
m3t4e9

Figure S2. Auditory sequences used in the experiment

The figure presents all the auditory sequences utilised in the experiment in musical notation. The memorised (M) sequences consisted of three sequences, each comprising the first five notes of the first three bars of the musical piece. These sequences (m1, m2, and m3) were presented nine times each, resulting in a total of 27 trials. The novel (N) sequences were generated through systematic variations of the three M sequences. This process involved altering every musical note in the sequence after the first (NT1), second (NT2), third (NT3), or fourth (NT4) note. Nine variations were created for each of the original M sequences across the four categories of N. This resulted in 27 N sequences for each category, totalling 108 N sequences. As illustrated in this figure, the variations were created according to the following rules: (i) Inverted melodic contours (used twice): the melodic contour of the variation was inverted in relation to the original M sequence (e.g., if the M sequence had the melodic contour: down-down-up-down, the N sequence would be: up-up-down-up); (ii) Same tone scrambled (used three times): the remaining notes of the M sequence were scrambled (e.g., M sequence: C-E-D-E-C was transformed into NT1 sequence: C-C-E-E-D). When this was not feasible (e.g., in the case of NT4, where only the last note differed from the M sequence), the last note of the M sequence was substituted with a random note; (iii) Same tone (used three times): the same note was repeatedly employed, sometimes varying only the octave (e.g., M sequence: C-E-D-E-C was changed to NT1 sequence: C-E8-E8-E8-E8); (iv) Scrambling intervals (used once): the intervals between the notes were scrambled (e.g., M sequence: 6thm – 2ndm – 2ndm – 3rdm was adapted to NT1 sequence: 2ndm, 6thm, 3rdm, 2ndm). In most cases, the harmonic structure of the N sequences in relation to the M sequences was preserved, with a few exceptions occurring for the 'inverted melodic contours' and 'scrambling intervals'. This strategy was employed to mitigate potential confounding variables arising from changes in harmony.

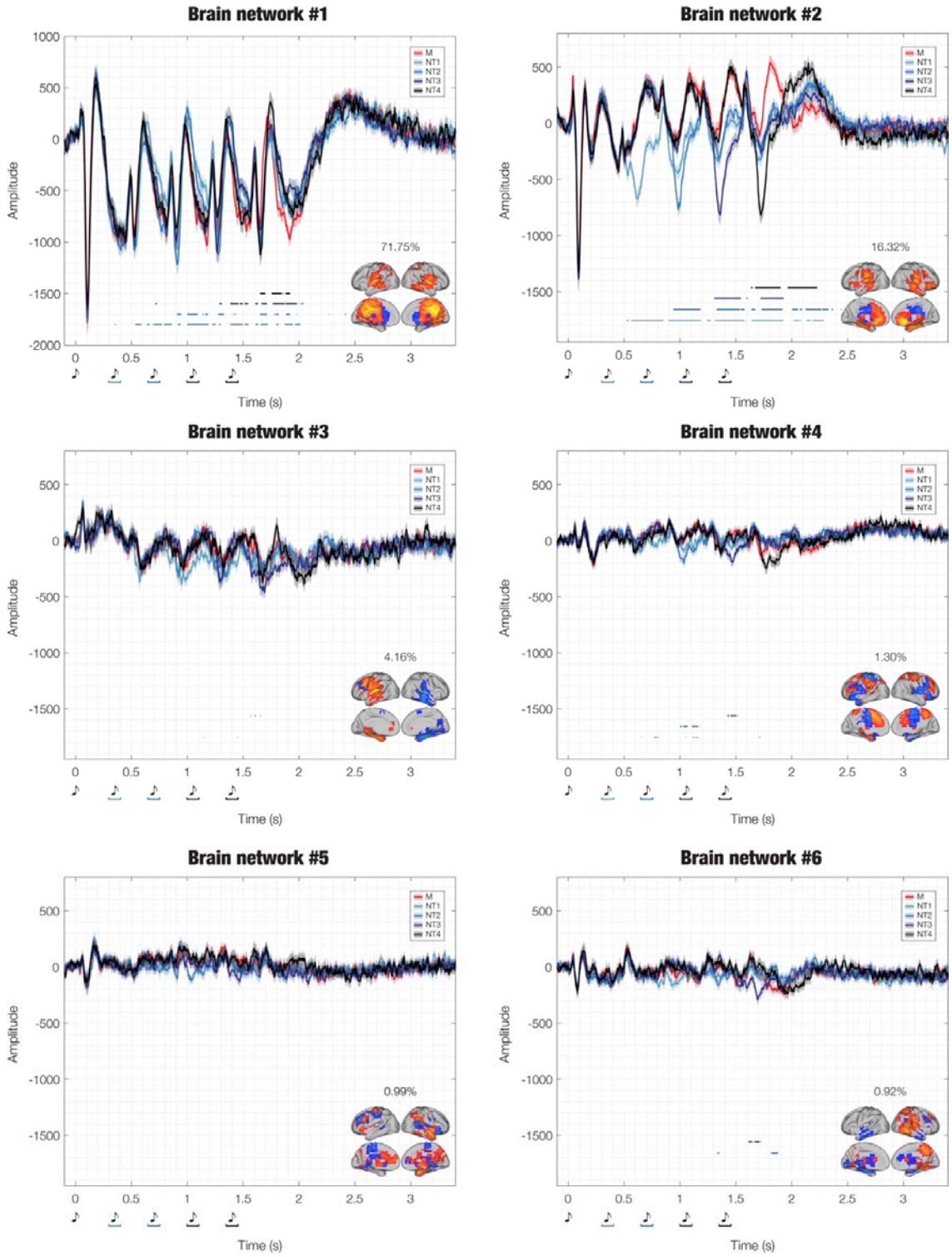
Brain network #1
Brain network #2
Brain network #3
Brain network #4
Brain network #5
Brain network #6
M
NT1
NT2
NT3
NT4
Amplitude
Time (s)
71.75%
16.32%
4.16%
1.30%
0.99%
0.92%

Figure S3: Time series and spatial activation patterns of significant brain networks according to the Monte-Carlo Simulations (MCS) approach

*This figure illustrates the time series and spatial activation patterns of brain networks that explained a higher variance than the first PCA component computed on time-wise randomised data (**Figure 3**), where both the order of brain voxels and time indices of the time series were disrupted. The variance explained by these surviving networks was: 71.75%, 16.32%, 4.16%, 1.30%, 0.99% and 0.92%, respectively. The figure shows that while six brain networks explained more variance than chance level (as determined by the randomised data), the first two brain networks accounted for most of the variance and displayed the clearest patterns in terms of differential brain activity between experimental conditions and spatial extent. As with the results shown in **Figure 1**, independent time series for each participant, brain network, and experimental condition were generated using PCA-derived weights from the averaged data. The individual time series were then averaged across participants, as shown in the plots. Shaded areas represent standard errors. The brain templates illustrate the spatial extent of the networks, with yellow voxels contributing the most and light blue voxels contributing the least to the time series. Only voxels with values exceeding the mean by more than one standard deviation in absolute terms are depicted. Blue-black lines indicate the temporal extent of the significant differences between M versus each category of N (i.e. M versus NT1, M versus NT2, M versus NT3, M versus NT4), computed using two-sided t-tests corrected for multiple comparisons via False Discovery Rate (FDR). Different shades of blue-black represent specific M versus N comparisons.*

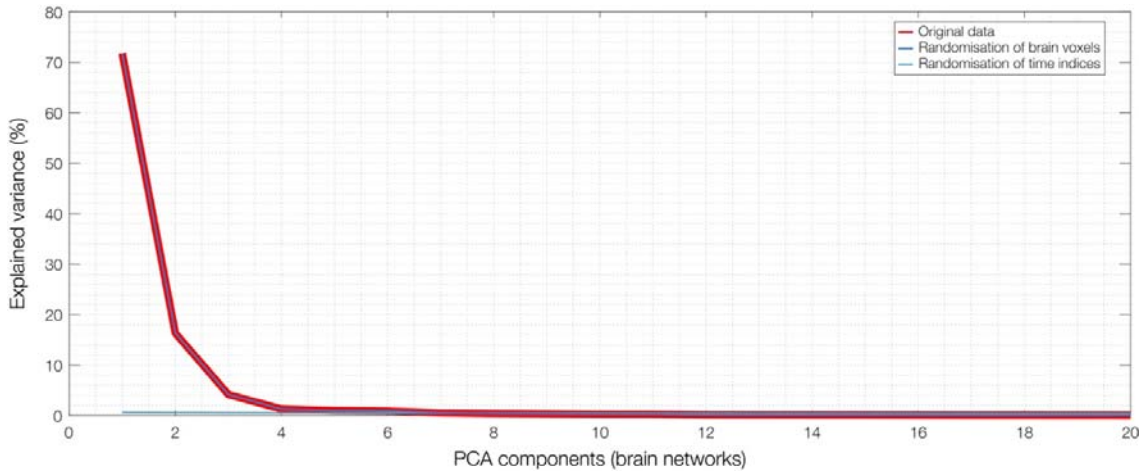

Figure S4: Variance explained by the top 20 principal component analysis (PCA) components for the original and randomised data

This figure illustrates the variance accounted for by the PCA components following analysis of the original data compared to the randomised data (both space randomisation and time randomisation). The results demonstrate that the variance explained by the original data and the space-randomised data remains identical. As shown in Figure 3, this randomisation impacted only the spatial activation patterns, without affecting the variance explained or the time series. In contrast, time randomisation led to a significant reduction in the variance explained by the top PCA components, alongside a disruption of both the spatial activation patterns of the brain networks and the time series.

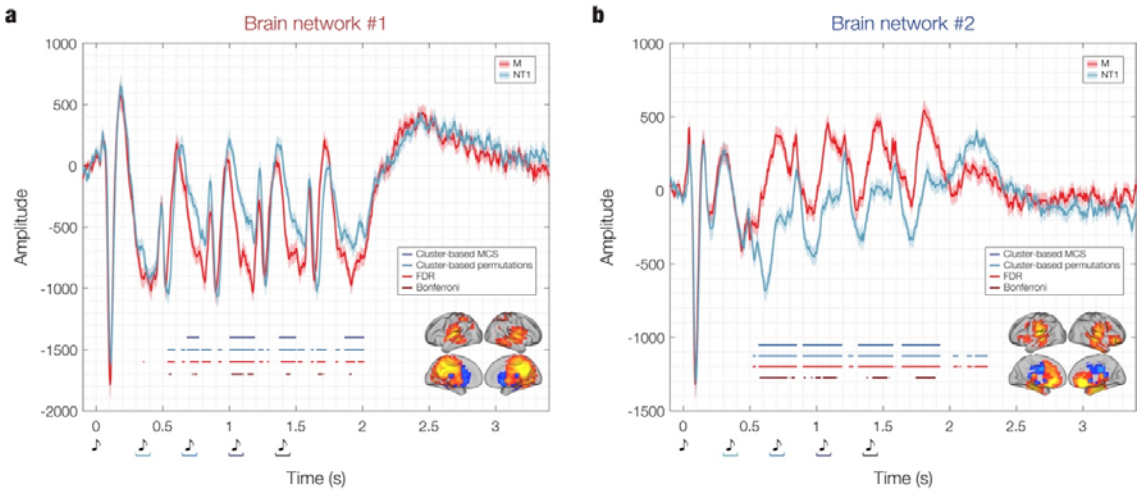

Figure S5: Multiple comparisons corrections

This figure presents an empirical comparison of four methods for correcting multiple comparisons. First, the plots illustrate the time series averaged across participants for each brain network and two experimental conditions (previously memorised and Novel T1 [NT1] sequences). Shaded areas represent standard errors. The brain templates illustrate the spatial extent of the networks, with yellow voxels contributing the most and light blue voxels contributing the least to the time series. Only voxels with values exceeding the mean by more than one standard deviation in absolute terms are depicted. Second, the plots highlight significant differences that survived various correction methods after contrasting previously memorised with NT1 sequences using two-sided t-tests for each time point and brain network. The methods compared are: (i) Bonferroni, (ii) False Discovery Rate (FDR), (iii) Cluster-based permutation test, and (iv) Cluster-based Monte Carlo Simulations (MCS). Bonferroni correction adjusts the significance level (α = .05) by dividing it by the number of tests performed, thereby reducing the likelihood of false positives. FDR ranks p-values from multiple tests, comparing them to the alpha level (α = .05) and identifying a stricter threshold (q) to control the proportion of false discoveries. The cluster-based permutation test, as described by Maris and Oostenveld[104], conducts statistical tests on the original data, identifies clusters of significant time points (α = .05), and performs 1000 permutations to shuffle labels and recalculate statistics. Clusters are deemed significant if their sizes exceed those from permuted data 99.9% of the time. Cluster-based MCS (MCS, α = .05, MCS p-value = .001), as detailed in our previous studies[7,105-111], identifies clusters of significant neighbouring time points (α = .05), performs 1000 permutations to randomise these values, and considers the clusters from the original data significant if they exceed 99.9% of the sizes of the ones obtained from the permuted data. The convergence of results across these methods further reinforces the robustness of the findings.

Supplementary Tables

The supplementary tables are available at the following link:
https://drive.google.com/drive/folders/10SOqFWYBwcZBBFb-N-L0hqaDL9620FaF?usp=sharing

Table S1. Statistical analysis of the two main brain networks

This table presents the results of statistical analyses conducted independently for the two brain networks that explained the highest variance. At each time point, t-tests compared memorised (M) versus each category of novel (NTs) sequences (i.e., M versus NT1, M versus NT2, M versus NT3, M versus NT4). Multiple comparisons were corrected using the false discovery rate (FDR) method. The table highlights significant time points along with the corresponding t-values.

Table S2. Statistical analysis of the two main brain networks obtained after randomisation of the data

This table presents the results of statistical analyses conducted independently for the two brain networks that explained the highest variance, separately for the two randomisation strategies adopted here: space randomisation and time randomisation. At each time point, t-tests compared memorised (M) versus each category of novel (NTs) sequences (i.e., M versus NT1, M versus NT2, M versus NT3, M versus NT4). Multiple comparisons were corrected using the false discovery rate (FDR) method. Significant time points and their corresponding t-values are reported.

Table S3. Comparison of significant results after different solutions for multiple comparisons correction

This table presents the empirical comparison of four methods for multiple comparisons correction. First, t-tests were conducted independently for each time point across the two main brain networks, contrasting memorised (M) versus each category of novel (NTs) sequences (i.e., M versus NT1, M versus NT2, M versus NT3, M versus NT4). Second, four different methods for multiple comparisons correction were employed: (i) Bonferroni, (ii) False Discovery Rate (FDR), (iii) cluster-based permutation test, and (iv) cluster-based Monte Carlo simulations (MCS). For Bonferroni and FDR corrections, the table displays significant time points along with their corresponding t-values. Regarding the cluster-based methods, significant clusters are reported, including cluster size, p-value, temporal extent of the cluster, and peak t-value within each cluster. These results are illustrated in ***Figure S3****.*

References

[1] Gazzaniga, M. S. (Ed.). *Handbook of cognitive neuroscience*. Springer. (2014). https://doi.org/10.1007/978-1-4899-2177-2

[2] Nobre, A. C. & Van Ede, F. Anticipated moments: temporal structure in attention. *Nat. Rev. Neurosci.* **19**, 34–48 (2017). https://doi.org/10.1038/nrn.2017.141

[3] Giraud, A.-L. & Poeppel, D. Cortical oscillations and speech processing: emerging computational principles and operations. *Nat. Neurosci.* **15**, 511–517 (2012). https://doi.org/10.1038/nrn.2017.141

[4] Lakatos, P., Karmos, G., Mehta, A. D., Ulbert, I. & Schroeder, C. E. Entrainment of Neuronal Oscillations as a Mechanism of Attentional Selection. *Science* **320**, 110–113 (2008). https://doi.org/10.1126/science.1154735

[5] Luck, S. J. (2014). *An Introduction to the Event-Related Potential Technique*, second edition. MIT Press.

[6] Cohen, M. X. A tutorial on generalized eigendecomposition for denoising, contrast enhancement, and dimension reduction in multichannel electrophysiology. *NeuroImage* **247**, 118809 (2022). https://doi.org/10.1016/j.neuroimage.2021.118809

[7] Bonetti, L., Fernández-Rubio, G., Carlomagno, F. et al. Spatiotemporal brain hierarchies of auditory memory recognition and predictive coding. *Nat. Commun.* **15,** 4313 (2024). https://doi.org/10.1038/s41467-024-48302-4

[8] Biswal, B., Yetkin, F. Z., Haughton, V. M., & Hyde, J. S. Functional connectivity in the motor cortex of resting human brain using echo planar mri. *Magn. Reson. Med.* **34**(4), 537–541. (1995). https://doi.org/10.1002/mrm.1910340409

[9] Sun, J. & Small, M. Unified framework for detecting phase synchronization in coupled time

series. *Phys. Rev.* **80**. (2009). https://doi.org/10.1103/PhysRevE.80.046219

[10] Ding, M., Chen, Y. and Bressler, S. L. Granger Causality: Basic Theory and Application to Neuroscience. In *Handbook of Time Series Analysis* (eds B. Schelter, M. Winterhalder and J. Timmer). (2006). https://doi.org/10.1002/9783527609970.ch17

[11] Vicente, R., Wibral, M., Lindner, M. & Pipa, G. Transfer entropy—a model-free measure of effective connectivity for the neurosciences. *J. Comput. Neurosci.* **30**, 45–67. (2010). https://doi.org/10.1007/s10827-010-0262-3

[12] Baccalá, L., Sameshima, K. Partial directed coherence: a new concept in neural structure determination. *Biol. Cybern.* **84**, 463–474 (2001). https://doi.org/10.1007/PL00007990

[13] Kamiński, M., Ding, M., Truccolo, W. *et al.* Evaluating causal relations in neural systems: Granger causality, directed transfer function and statistical assessment of significance. *Biol. Cybern.* **85**, 145–157 (2001). https://doi.org/10.1007/s004220000235

[14] Nolte, G. *et al.* Robustly Estimating the Flow Direction of Information in Complex Physical Systems. *Phys. Rev. Lett.* **100**, (2008). https://doi.org10.1103/PhysRevLett.100.234101

[15] Friston, K., Harrison, L., & Penny, W. Dynamic causal modelling. *NeuroImage*, **19**(4), 1273–1302. (2003). https://doi.org/10.1016/s1053-8119(03)00202-7

[16] Bullmore, E., & Sporns, O. Complex brain networks: graph theoretical analysis of structural and functional systems. *Nat. Rev. Neurosci.* **10**, 186–198. (2009). https://doi.org/10.1038/nrn2575

[17] Seedat, Z. A. et al. Mapping Interictal activity in epilepsy using a hidden Markov model: A magnetoencephalography study. *Hum. Brain Mapp.* **44**(1), 66–81. (2022). https://doi.org/10.1002/hbm.26118

[18] Cabral, J., et al. Cognitive performance in healthy older adults relates to spontaneous switching between states of functional connectivity during rest. *Sci. Rep.* **7**, 5135. (2017). https://doi.org/10.1038/s41598-017-05425-7

[19] Cichy, R. M., & Pantazis, D. Multivariate pattern analysis of MEG and EEG: A comparison of representational structure in time and space. *NeuroImage* **158**, 441–454. (2017). https://doi.org/10.1016/j.neuroimage.2017.07.023

[20] King, J. & Dehaene, S. Characterizing the dynamics of mental representations: the temporal generalization method. *Trends Cogn. Sci.* **18**, 203–210. (2014). https://doi.org/10.1016/j.tics.2014.01.002

[21] Carbonell, F., Bellec, P. & Shmuel, A. Global and system-specific resting-state fMRI fluctuations are uncorrelated: principal component analysis reveals anti-correlated networks. *Brain Connect*. **1**, 496–510. (2011). https://doi.org/10.1089/brain.2011.0065

[22] Greicius, M. D., Srivastava, G., Reiss, A. L. & Menon, V. Default-mode network activity distinguishes Alzheimer's disease from healthy aging: evidence from functional MRI. *Proc. Natl. Acad. Sci. U. S. A.*, **101**, 4637–4642. (2004). https://doi.org/10.1073/pnas.0308627101

[23] Mantini, D., Perrucci, M. G., Del Gratta, C., Romani, G. L. & Corbetta, M. Electrophysiological signatures of resting state networks in the human brain. *Proc. Natl. Acad. Sci. U. S. A.* **104**, 13170–13175. (2007). https://doi.org/10.1073/pnas.0700668104

[24] Timmermann, C. et al. Human brain effects of DMT assessed via EEG-fMRI. *PNAS* **120**, e2218949120 (2023). https://doi.org/10.1073/pnas.2218949120

[25] Zhong, Y. et al. Detecting functional connectivity in fMRI using PCA and regression analysis. *Brain Topogr*. **22**, 134–144. (2009). https://doi.org/10.1007/s10548-009-0095-4

[26] Bahrami, M., Laurienti, P. J., Shappell, H. M., & Simpson, S. L. Brain Network Analysis: A Review on Multivariate Analytical Methods. *Brain Connect*. **13**(2), 64–79. (2023). https://doi.org/10.1089/brain.2022.0007

[27] Amaro, E., & Barker, G. J. Study design in fMRI: Basic principles. *Brain Cogn*. **60**(3), 220–232. (2006). https://doi.org/10.1016/j.bandc.2005.11.009

[28] Ruchkin, D. S., Villegas, J. & John, E. R. An Analysis of Average Evoked Potentials Making
use of Least Mean Square Techniques. *Ann. N. Y. Acad. Sci.* **115**, 799–826 (1964). https://doi.org/10.1111/j.1749-6632.1964.tb50665.x

[29] Donchin, E. A Multivariate Approach to the Analysis of Average Evoked Potentials. *IEEE Trans. Biomed. Eng*. **13**, 131–139 (1966). https://doi.org/10.1109/tbme.1966.4502423

[30] Duffy, F. H., Jones, K., Bartels, P., McAnulty, G. & Albert, M. Unrestricted principal components analysis of brain electrical activity: Issues of data dimensionality, artifact, and utility. *Brain Topogr*. **4**, 291–307 (1992). https://doi.org/10.1007/bf01135567

[31] Picton, T. W. et al. Guidelines for using human event related potentials to study cognition:
Recording standards and publication criteria. *Psychophysiology* **37**, 127–152 (2000). https://doi.org/10.1111/1469-8986.3720127

[32] Dien J, & Frishkoff, G. A. Principal components analysis of event-related potential datasets.
In: Event-related potentials: a methods handbook (Handy T. C., ed), pp 189–208. Cambridge: MIT Press. (2005).

[33] Dien, J. Applying Principal Components Analysis to Event-Related Potentials: A Tutorial. *Dev. Neuropsychol*. **37**, 497–517 (2012). https://doi.org/10.1080/87565641.2012.697503

[34] Foti, D., Weinberg, A., Dien, J., & Hajcak, G. (2011). Event related potential activity in the basal ganglia differentiates rewards from nonrewards: Temporospatial principal components analysis and source localization of the feedback negativity. *Hum. Brain Mapp.* **32**(12), 2207-2216. https://doi.org/10.1002/hbm.21182

[35] Kayser, J., & Tenke, C. E. Optimizing PCA methodology for ERP component identification and measurement: theoretical rationale and empirical evaluation. *Clin. Neurophysiol. Pract.* **114**(12), 2307–2325. (2003). https://doi.org/10.1016/s1388-2457(03)00241-4

[36] Brookes, M. J. et al. Investigating the electrophysiological basis of resting state networks using magnetoencephalography. *Proc. Natl. Acad. Sci. U. S. A.* **108**, 16783–16788 (2011). https://doi.org/10.1073/pnas.1112685108

[37] Rosso, M., Fernández-Rubio, G. Keller, P., Brattico, E., Vuust, P., Kringelbach, M. L., Bonetti, L. FREQuency-resolved brain Network Estimation via Source Separation (FREQ-NESS). (2024). Biorxiv, https://www.biorxiv.org/content/10.1101/2024.08.28.610155.full.pdf

[38] Rosso, M., Moens, B., Leman, M. & Moumdjian, L. Neural entrainment underpins sensorimotor synchronization to dynamic rhythmic stimuli. *NeuroImage* **277**, 120226 (2023). https://doi.org/10.1016/j.neuroimage.2023.120226

[39] Rosso, M., Heggli, O. A., Maes, P. J., Vuust, P. & Leman, M. Mutual beta power modulation in dyadic entrainment. *NeuroImage* **257**, 119326 (2022). https://doi.org/10.1016/j.neuroimage.2022.119326

[40] Rosso, M., Leman, M. & Moumdjian, L. Neural Entrainment Meets Behavior: The Stability
Index as a Neural Outcome Measure of Auditory-Motor Coupling. *Front. Hum. Neurosci.* **15**. (2021). https://doi.org/10.3389/fnhum.2021.668918

[41] Zuure, M. B., Hinkley, L. B., Tiesinga, P. H. E., Nagarajan, S. S. & Cohen, M. X. Multiple Midfrontal Thetas Revealed by Source Separation of Simultaneous MEG and EEG. *J. Neurosci.* **40**, 7702–7713. (2020). https://doi.org/10.1016/j.jneumeth.2020.109063

[42] Cohen, M. X. & Gulbinaite, R. Rhythmic entrainment source separation: Optimizing analyses of neural responses to rhythmic sensory stimulation. *NeuroImage* **147**, 43–56. (2017). https://doi.org/10.1016/j.neuroimage.2016.11.036

[43] Deco, G., Tononi, G., Boly, M. & Kringelbach, M. L. Rethinking segregation and integration: contributions of whole-brain modelling. *Nat. Rev. Neurosci*. **16**, 430–439 (2015). https://doi.org/10.1038/nrn3963

[44] Deco, G. et al. Single or multiple frequency generators in on-going brain activity: A mechanistic whole- brain model of empirical MEG data. *Neuroimage* **152**, 538–550 (2017). https://doi.org/10.1016/j.neuroimage.2017.03.023

[45] Hansen, E. C. A., Battaglia, D., Spiegler, A., Deco, G. & Jirsa, V. K. Functional connectivity dynamics: modeling the switching behavior of the resting state. *Neuroimage* **105**, 525–535 (2015). https://doi.org/10.1016/j.neuroimage.2014.11.001

[46] Zhang, Z. *et al.* Resting-state brain organization revealed by functional covariance networks. *PLoS One* **6**, e28817 (2011). https://doi.org/10.1371/journal.pone.0028817

[47] Winkler, I. & Cowan, N. From Sensory to Long-Term Memory. *Exp. Psychol.* **52**, 3–20 (2005). https://doi.org/10.1027/1618-3169.52.1.3

[48] Otten, L. J. & Donchin, E. Relationship between P300 amplitude and subsequent recall for distinctive events: Dependence on type of distinctiveness attribute. *Psychophysiology* **37**, 644–661 (2000). https://doi.org/10.1111/1469-8986.3750644

[49] Winkler, I. Interpreting the Mismatch Negativity. *J. Psychophysiol.* **21**, 147–163 (2007). https://doi.org/10.1027/0269-8803.21.34.147

[50] Fitzgerald, K. & Todd, J. Making Sense of Mismatch Negativity. *Front. Psychiatry* **11**, (2020). https://doi.org/10.3389/fpsyt.2020.00468

[51] Mulert, C. et al. Auditory cortex and anterior cingulate cortex sources of the early evoked gamma-band response: Relationship to task difficulty and mental effort. *Neuropsychologia* **45**, 2294–2306 (2007). https://doi.org/10.1016/j.neuropsychologia.2007.02.020

[52] Luan, Y., Wang, C., Jiao, Y. et al. Abnormal functional connectivity and degree centrality in anterior cingulate cortex in patients with long-term sensorineural hearing loss. *Brain Imaging Behav*. **14**, 682–695 (2020). https://doi.org/10.1007/s11682-018-0004-0

[53] Yukie, M. Neural connections of auditory association cortex with the posterior cingulate cortex in the monkey. *Neurosci. Res.* **22**, 179–187 (1995). https://doi.org/10.1016/0168-0102(95)00888-1

[54] Tzourio, N. et al. Functional Anatomy of Human Auditory Attention Studied with PET. *NeuroImage* **5**, 63–77 (1997). https://doi.org/10.1006/nimg.1996.0252

[55] Crottaz-Herbette, S. & Menon, V. Where and When the Anterior Cingulate Cortex Modulates Attentional Response: Combined fMRI and ERP Evidence. *J. Cogn. Neurosci.* **18**, 766–780 (2006). https://doi.org/10.1162/jocn.2006.18.5.766

[56] Pugh, K. R. et al. Auditory Selective Attention: An fMRI Investigation. *NeuroImage* **4**, 159–173 (1996). https://doi.org/10.1006/nimg.1996.0067

[57] Kumar, S. et al. Representations of specific acoustic patterns in the auditory cortex and hippocampus. *Proc. R. Soc. Lond. B Biol. Sci.* **281**, 20141000 (2014). https://doi.org/10.1098/rspb.2014.1000

[58] Dürschmid, S. et al. Hierarchy of prediction errors for auditory events in human temporal and frontal cortex. *PNAS* **113**, 6755–6760 (2016). https://doi.org/10.1098/rspb.2014.1000

[59] Casado-Román, L., Carbajal, G. V., Pérez-González, D. & Malmierca, M. S. Prediction error signaling explains neuronal mismatch responses in the medial prefrontal cortex. *PLoS Biol*. **18**, e3001019 (2020). https://doi.org/10.1371/journal.pbio.3001019

[60] Plakke, B. & Romanski, L. M. Auditory connections and functions of prefrontal cortex. *Front. Neurosci.* **8** (2014). https://doi.org/10.3389/fnins.2014.00199

[61] Nieto-Castanon, A., Ghosh, S. S., Tourville, J. A. & Guenther, F. H. Region of interest based analysis of functional imaging data. *NeuroImage* **19**, 1303–1316 (2003). https://doi.org/10.1016/S1053-8119(03)00188-5

[62] Padilla-Buritica, J. I., Martinez-Vargas, J. D. & Castellanos-Dominguez, G. Emotion Discrimination Using Spatially Compact Regions of Interest Extracted from Imaging EEG Activity. *Front. Comp. Neurosci.* **10**, (2016). https://doi.org/10.3389/fncom.2016.00055

[63] Mamashli, F., Hämäläinen, M., Ahveninen, J. *et al*. Permutation Statistics for Connectivity Analysis between Regions of Interest in EEG and MEG Data. *Sci. Rep.* **9**, 7942 (2019). https://doi.org/10.1038/s41598-019-44403-z

[64] Marwan, N., Carmenromano, M., Thiel, M. & Kurths, J. Recurrence plots for the analysis of complex systems. *Phys. Rep.* **438**, 237–329 (2007). https://doi.org/10.1016/j.physrep.2006.11.001

[65] Bradley, E. & Kantz, H. Nonlinear time-series analysis revisited. *Chaos an Interdisciplinary Journal of Nonlinear Science* **25** (2015). https://doi.org/10.1063/1.4917289

[66] Ruchkin, D. S., Villegas, J. & John, E. R. An Analysis of Average Evoked Potentials Making
use of Least Mean Square Techniques. *Ann. N. Y. Acad. Sci.* **115**, 799–826 (1964). https://doi.org/10.1111/j.1749-6632.1964.tb50665.x

[67] Picton, T. W. et al. Guidelines for using human event related potentials to study cognition:
Recording standards and publication criteria. *Psychophysiology* **37**, 127–152 (2000). https://doi.org/10.1111/1469-8986.3720127

[68] Dien J, & Frishkoff, G. A. Principal components analysis of event-related potential datasets.
In: Event-related potentials: a methods handbook (Handy T. C., ed), pp 189–208. Cambridge: MIT Press. (2005).

[69] Dien, J. Applying Principal Components Analysis to Event-Related Potentials: A Tutorial. *Dev. Neuropsychol.* **37**, 497–517 (2012). https://doi.org/10.1080/87565641.2012.697503

[70] Donchin, E. A Multivariate Approach to the Analysis of Average Evoked Potentials. *IEEE Trans. Biomed. Eng.* **13**, 131–139 (1966). https://doi.org/10.1109/tbme.1966.4502423

[71] Duffy, F. H., Jones, K., Bartels, P., McAnulty, G. & Albert, M. Unrestricted principal components analysis of brain electrical activity: Issues of data dimensionality, artifact, and utility. *Brain Topogr*. **4**, 291–307 (1992). https://doi.org/10.1007/bf01135567

[72] Kayser, J., & Tenke, C. E. Optimizing PCA methodology for ERP component identification and measurement: theoretical rationale and empirical evaluation. *Clin. Neurophysiol. Pract.* **114**(12), 2307–2325. (2003). https://doi.org/10.1016/s1388-2457(03)00241-4

[73] McKeown, M. J. & Sejnowski, T. J. Independent component analysis of fMRI data: examining the assumptions. *Hum. Brain Mapp.* **6**, 368–372 (1998). https://doi.org/10.1002/(SICI)1097-0193(1998)6:5/6<368::AID-HBM7>3.0.CO;2-E

[74] Leonardi, N. *et al*. Principal components of functional connectivity: a new approach to study dynamic brain connectivity during rest. *Neuroimage* **83**, 937–950 (2013). https://doi.org/10.1016/j.neuroimage.2013.07.019

[75] McKeown, M. J. *et al*. Spatially independent activity patterns in functional MRI data during the Stroop color-naming task. *PNAS* **95**, 803–810 (1998). https://doi.org/10.1073/pnas.95.3.803

[76] Scharf, F., Widmann, A., Bonmassar, C. & Wetzel, N. A tutorial on the use of temporal principal component analysis in developmental ERP research – Opportunities and challenges. *Dev. Cogn. Neurosci.* **54**, 101072 (2022). https://doi.org/10.1016/j.dcn.2022.101072

[77] Taulu, S. & Simola, J. Spatiotemporal signal space separation method for rejecting nearby interference in MEG measurements. *Phys. Med. Biol.* **51**, 1759–1768 (2006). https://doi.org/10.1088/0031-9155/51/7/008

[78] Woolrich, M., Hunt, L., Groves, A. & Barnes, G. MEG beamforming using Bayesian PCA for adaptive data covariance matrix regularization. *Neuroimage* **57**, 1466–1479 (2011). https://doi.org/10.1016/j.neuroimage.2011.04.041

[79] Oostenveld, R., Fries, P., Maris, E. & Schoffelen, J.-M. FieldTrip: open source software for advanced analysis of MEG, EEG, and invasive electrophysiological data. *Comput. Intell. Neurosci.* **2011**, 1–9 (2011). https://doi.org/10.1155/2011/156869

[80] Woolrich, M. W. et al. Bayesian analysis of neuroimaging data in FSL. *Neuroimage* **45**, S173–S186 (2009). https://doi.org/10.1016/j.neuroimage.2008.10.055

[81] Penny, W. D., Friston, K. J., Ashburner, J. T., Kiebel, S. J. & Nichols, T. E. *Statistical parametric mapping: the analysis of functional brain images*. Elsevier. (2011).

[82] Mantini, D. et al. A signal-processing pipeline for magnetoencephalography resting-state networks. *Brain Connect.* **1**, 49–59 (2011). https://doi.org/10.1089/brain.2011.0001

[83] Wang, G., Teng, C., Li, K., Zhang, Z. & Yan, X. The Removal of EOG Artifacts From EEG Signals Using Independent Component Analysis and Multivariate Empirical Mode Decomposition. *IEEE J. Biomed. Health Inform.* **20**, 1301–1308 (2015). https://doi.org/10.1109/JBHI.2015.2450196

[84] Huang, M., Mosher, J. C. & Leahy, R. A sensor-weighted overlapping-sphere head model and exhaustive head model comparison for *MEG. Phys. Med. Biol.* **44**, 423 (1999). https://doi.org/10.1088/0031-9155/44/2/010

[85] Nolte, G. The magnetic lead field theorem in the quasi-static approximation and its use for magnetoencephalography forward calculation in realistic volume conductors. *Phys. Med. Biol*. **48**, 3637–3652 (2003). https://doi.org/10.1088/0031-9155/48/22/002

[86] Brookes, M. J. et al. Beamformer reconstruction of correlated sources using a modified source model. *Neuroimage* **34**, 1454–1465 (2007). https://doi.org/10.1016/j.neuroimage.2006.11.012

[87] Gross, J. et al. Good practice for conducting and reporting MEG research. *Neuroimage* **65**, 349–363 (2013). https://doi.org/10.1016/j.neuroimage.2012.10.001

[88] Hillebrand, A. & Barnes, G. R. Beamformer analysis of MEG data. *Int. Rev. Neurobiol.* **68**, 149–171 (2005). https://doi.org/10.1016/S0074-7742(05)68006-3

[89] Afnan, J. et al. Validating MEG source imaging of resting state oscillatory patterns with an intracranial EEG atlas. *Neuroimage* **274**, 120158 (2023). https://doi.org/10.1016/j.neuroimage.2023.120158

[90] Sauseng, P., Griesmayr, B., Freunberger, R. & Klimesch, W. Control mechanisms in working memory: a possible function of EEG theta oscillations. *Neurosci. Biobehav Rev.* **34**, 1015–1022 (2010). https://doi.org/10.1016/j.neubiorev.2009.12.006

[91] Hall, E. L., Woolrich, M.W., Thomaz, C.E., Morris, P.G. & Brookes, M. J. Using variance information in magnetoencephalography measures of functional connectivity. *Neuroimage* **67**, 203–212 (2013). https://doi.org/10.1016/j.neuroimage.2012.11.011

[92] Luckhoo, H. T., Brookes, M. J. & Woolrich, M. W. Multi-session statistics on beamformed MEG data. *Neuroimage* **95**, 330–335 (2014). https://doi.org/10.1016/j.neuroimage.2013.12.026

[93] Van Veen, B. D., van Drongelen, W., Yuchtman, M. & Suzuki, A. Localization of brain electrical activity via linearly constrained minimum variance spatial filtering. *IEEE Trans. Biomed. Eng.* **44**, 867–880 (1997). https://doi.org/10.1109/10.623056

[94] Haufe, S. *et al.* On the interpretation of weight vectors of linear models in multivariate neuroimaging. *NeuroImage* **87**, 96–110 (2013). https://doi.org/10.1016/j.neuroimage.2013.10.067

[95] Maris, E. & Oostenveld, R. Nonparametric statistical testing of EEG- and MEG-data. *J. Neurosci. Methods* **164**, 177–190 (2007). https://doi.org/10.1016/j.jneumeth.2007.03.024

[96] Bonetti, L., Fernández-Rubio, G., Lumaca, M. *et al.* Age-related neural changes underlying long-term recognition of musical sequences. *Commun Biol* **7**, 1036 (2024). https://doi.org/10.1038/s42003-024-06587-7

[97] Bonetti, L. *et al.* Spatiotemporal whole-brain activity and functional connectivity of melodies recognition. *Cerebr. Cortex* **34**, (2024). https://doi.org/10.1093/cercor/bhae320

[98] Bonetti, L. *et al.* Brain recognition of previously learned versus novel temporal sequences: a differential simultaneous processing. *Cerebr. Cortex* **33**, 5524–5537 (2022). https://doi.org/10.1093/cercor/bhac439

[99] Fernández-Rubio, G., Brattico, E., Kotz, S.A. *et al.* Magnetoencephalography recordings reveal the spatiotemporal dynamics of recognition memory for complex versus simple

auditory sequences. *Commun. Biol.* **5**, 1272 (2022). https://doi.org/10.1038/s42003-022-04217-8

[100] Fernández-Rubio, G., Carlomagno, F., Vuust, P., Kringelbach, M. L. & Bonetti, L. Associations between abstract working memory abilities and brain activity underlying long-term recognition of auditory sequences. *PNAS Nexus* 1, (2022). https://doi.org/10.1093/pnasnexus/pgac216

[101] Hoegholt, N. F. *et al.* A magnetoencephalography study of first-time mothers listening to infant cries. *Cerebr. Cortex* **33**, 5896–5905 (2022). https://doi.org/10.1093/cercor/bhac469

[102] Bonetti, L. *et al.* Moderate associations between BDNF Val66Met gene polymorphism, musical expertise, and mismatch negativity. *Heliyon* **9**, e15600 (2023). https://doi.org/10.1016/j.heliyon.2023.e15600

[103] Bonetti, L. et al. Spatiotemporal brain hierarchies of auditory memory recognition and predictive coding [Dataset]. *Zenodo.* (2024). https://doi.org/10.5281/zenodo.10715160

[104] Maris, E. & Oostenveld, R. Nonparametric statistical testing of EEG- and MEG-data. *J. Neurosci. Methods* **164**, 177–190 (2007). https://doi.org/10.1016/j.jneumeth.2007.03.024

[105] Bonetti, L., Fernández-Rubio, G., Lumaca, M. *et al.* Age-related neural changes underlying long-term recognition of musical sequences. *Commun Biol* **7**, 1036 (2024). https://doi.org/10.1038/s42003-024-06587-7

[106] Bonetti, L. *et al.* Spatiotemporal whole-brain activity and functional connectivity of melodies recognition. *Cerebr. Cortex* **34**, (2024). https://doi.org/10.1093/cercor/bhae320

[107] Bonetti, L. *et al.* Brain recognition of previously learned versus novel temporal sequences: a differential simultaneous processing. *Cerebr. Cortex* **33**, 5524–5537 (2022). https://doi.org/10.1093/cercor/bhac439

[108] Fernández-Rubio, G., Brattico, E., Kotz, S.A. *et al.* Magnetoencephalography recordings reveal the spatiotemporal dynamics of recognition memory for complex versus simple auditory sequences. *Commun. Biol.* **5**, 1272 (2022). https://doi.org/10.1038/s42003-022-04217-8

[109] Fernández-Rubio, G., Carlomagno, F., Vuust, P., Kringelbach, M. L. & Bonetti, L. Associations between abstract working memory abilities and brain activity underlying long-term recognition of auditory sequences. *PNAS Nexus* 1, (2022). https://doi.org/10.1093/pnasnexus/pgac216

[110] Hoegholt, N. F. *et al.* A magnetoencephalography study of first-time mothers listening to infant cries. *Cerebr. Cortex* **33**, 5896–5905 (2022). https://doi.org/10.1093/cercor/bhac469

[111] Bonetti, L. *et al.* Moderate associations between BDNF Val66Met gene polymorphism, musical expertise, and mismatch negativity. *Heliyon* **9**, e15600 (2023). https://doi.org/10.1016/j.heliyon.2023.e15600